J Indian Inst Sci, Jan–Feb 1992, 72, 35-91

IISc THESES ABSTRACTS

Thesis Abstract (Ph.D.)

Boundary restraint effects and correction rules for two-dimensional separated flow past bodies by J. Deenadhayalan.
Research supervisor: G. N. V. Rao.
Department: Aerospace Engineering

1. Introduction

It is now recognized[1-3] that considerable uncertainties and inadequacies exist in methods for effecting blockage or boundary-restraint corrections in wind and water tunnels. These factors have led to search for other approaches such as Adaptive wall method[3], Boundary measurement methods[1,3] and Momentum balance method[2].

In this work, studies of the effect of solid and free-jet boundaries in two-dimensional separated flows have been made using free-streamline theory, modelled to yield flows closer to reality than those in the pioneering work of Kirchhoff and Helmholtz. The models employed are Momentum surface model[4] and Displacement surface model[5]. Solid, free-jet and partially open solid boundaries have been considered.

2. Results and discussion

Studies have shown that modelling plays a vital role in predicting blockage effects, even when both the models are quite realistic. In the Displacement surface model, at large blockages, the forces and moment coefficients acting on a body increase with increase of blockage, at the same back-pressure coefficient, whereas in the Momentum surface model, just the opposite trend has been observed in the aerodynamic coefficients, in a closed jet tunnel. Also, the separated flows past bodies in the case of a free jet issuing from a solid nozzle and as a free jet which is doubly infinite in length have been studied using Displacement surface model.

These studies confirm that even in separated flows past bodies in completely closed and completely open-jet tunnels, opposite trends of blockage are observed as in the case of attached flows.

Following these analyses, it was conjectured that a suitable combination of rigid and open-jet boundaries in a tunnel wall can yield a blockage-free separated flow. The suppression of boundary-restraint effects is shown to be feasible for a particular value of the partial opening of the solid wall and the pressure at the opening. It is observed that in all cases, the back pressure in the near-wake separation bubble occurs as an unknown parameter, which can, in principle, have any value in the tunnel model and in unbounded fluid flow, unless additional restraints are imposed to enable a unique relation between the two to exist. One such is obviously to require that the flow separation in both the conditions be a boundary-layer separation. In the inviscid domain, other restraints are suggested to obtain a unique relation between the back pressures on the model in a tunnel and in unbounded fluid when back pressures are arbitrary, the correction procedure has to be semi-empirical, in which case, two such methods are proposed, somewhat similar to those upon which Reynolds number corrections for drag and lift are made in airfoil experiments. Apart from these, brief reviews of the development of free streamline theory for separated flows and the development of the existing boundary correction methods have been presented.

References

1 ASHILL, P R AND KEATING, R F A — Calculation of tunnel wall interference from wall pressure measurements, *RAE Tech Rep* 85086, 1985

2 MASKELL, E C — A theory of the blockage effects on bluff bodies and stalled wings in a closed wind tunnel, *ARC R and M* 3400, 1963

3 NEWMAN, P A AND BARNWELL, R W — *Wind tunnel wall interference assessment/correction*, NASA Conf Publ No 2319, Jan 1983

4 OBA, R — A study on finite supercavitating blocked flow, *Rep Inst High Speed Mech*, Japan, 1968/69, **20**, 345–371

5 SATO, K — Nonlinear analysis of cavity flows around arbitrarily shaped bodies in a constrained flow, *J Fluid Mech*, 1982, **125**, 347–358

Thesis Abstract (Ph.D.)

Studies on hypergolic ignition of solid fuel–liquid oxidizer systems by K. N. Murthy. Research supervisor: S. R. Jain.
Department: Aerospace Engineering.

1. Introduction

The exciting achievements of space science and technology owe much to the development of suitable propellants as source of propulsion energy in rocket engines. Of the various types of propellants, the technology of the composite solid propellants, and also of the bihquid propellants, has been more or less well established over the years There is still another class of propellants, known as hybrid propeliants, comprising a combination of a solid fuel and a liquid oxidizer, that has not made the same progress in rocketry, although it offers many distinct advantages The full advantage of a hybrid propeliant system, however, is realized by making use of a hypergolic combination of fuel and oxidizer In such a combination, self-ignition of the propellant results when the two components are simply brought in contact with each other One of the prime considerations in these systems is the evolution of fuel–oxidizer systems having shortest possible ignition delays (IDs) to avoid devastating pressure spikes which are generated on delayed ignition leading to 'hard start' or even destruction of the rocket motor

By using exotic fuel–oxidizer systems like liquid, fluorine and metal hydride, very low ID can be achieved, but the practical problems associated with stability, handling and toxic nature of these materials prohibit their use in real applications Commonly used fuel and oxidizer combinations, on the other hand, give longer ignition delays It is apparent, therefore, that the low profile of hybrid systems in rocket technology is mainly due to lack of suitable highly hypergolic fuel–oxidizer combinations In recent years, several attempts have been made[1–3] to evolve hypergolic systems for hybrid rockets. However, in most of the studies, ignition delays reported have been determined by taking the fuel in powder form Since, in actual applications, the fuel is usually taken in a 'grain' form the ignition delay data on the cast fuel grains are more relevant Usually, ignition delay increases on casting the fuel, hence, it is essential that the binder chosen imparts the required mechanical strength to the grain without significantly increasing the ignition delay The present research is aimed at understanding the phenomena relating to the onset of ignition in hypergolic systems, and makes an attempt to develop novel metallized hypergolic systems having short ignition delays and high theoretical rocket performance

2. Experimental

A large number of solid fuels, like Schiff bases, azines, hydrazones, thiosemicarbazones, mono- and bis-thiocarbonohydrazones, hydroxy compounds, aromatic hydrocarbons, etc., have been investigated for their hypergolicity with white or red fuming nitric acid (WFNA or RFNA) as oxidizer. The ignition delays of

these systems have been determined using a droptester-type device at room temperature. The effect of addition of metal powders to the fuels on the ID has been determined Differential thermal analysis of the various compounds prepared during the course of the present study has been carried out to characterize and ascertain their thermal stability The preignition-quenched products in a few cases have been identified by chemical analysis Special binders have been synthesized for casting the promising fuels into grains

The heat of combustion of various hypergolic systems with HNO_3 as oxidizer has been measured in a modified combustion calorimeter described earlier A novel experimental set-up has been devised for recording the transient temperature of the hypergolic systems It involves measuring the resistance of a micron-thin platinum film deposited in a glass crucible, capturing the data on a digital oscilloscope and processing them on a computer Necessary hardware and software for these measurements have been developed The theoretical performance rocket parameters of the various propellant systems have been obtained on a DEC-1090 computer using the NASA-SP 273 program

3. Results and conclusions

A variety of solid organic compounds, such as Schiff bases, azines, hydrazones, thiocarbonohydrazones, thiosemicarbazones, hydroxy compounds and certain elements like carbon and phosphorus, on mixing with metal powders, specially with magnesium, become synergistically hypergolic with WFNA In the absence of magnesium powder, these compounds are either nonhypergolic or have longer ignition delays. The synergistic ignition behavior has been explained in terms of increased exothermicity of the system, primarily due to the heat-evolving chemical reactions occurring between the fuel and the oxidizer, in the preignition stage Nitration has been established as one of the important preignition reactions by the identification of 3-nitrocatechol in catechol-Mg-WFNA system

The ignition delay of several solid hypergolic fuel compositions, cast using various polymeric binders, or as melts, has been determined with WFNA as oxidizer The ignition delay increases drastically on casting with binders like carboxyl or hydroxyl-terminated polybutadienes Fuel grains cast using some newly synthesized epoxy resins are found to have short ignition delays, of the order of 200 ms, and also good mechanical strength Increasing the amount of binder in the composition retards the hypergolicity of the grain Low-melting hypergolic compounds have been used for melt-casting fuel powders. The ignition delays of the melt-cast grains are longer than those determined by taking the composition in powder form. The effect of highly hypergolic additives and metal powders on the ignition delay of the cast compositions has been determined. Grains having good mechanical strength and short ignition delays have been obtained by optimizing the fuel grain composition

The heat of combustion with WFNA as oxidizer of various hypergolic systems has been measured. An evaluation of the performance parameters reveals that these systems have specific impulse (vacuum) of the order of 280 s at chamber pressure, 30 atm, with expansion ratio, 60. The maximum specific impulse is obtained at the same fuel composition at which the minimum ignition delay is observed. Of the various systems studied, the Schiff base–Mg–WFNA systems appear to be most promising. The results have been explained in terms of the physico-chemical processes occurring in these systems.

A novel experimental set-up has been developed for recording the temperature history of hypergolic propellant systems which ignite in milli-seconds time intervals Biliquid propellant systems are found to give better profile reproducibility than hybrid systems In furfurylalcohol–aniline–WFNA systems, the slope of the profile and the surface temperature recorded at ignition point are found to be related to the ignition delays of the system, the steeper the slope and lower the surface temperature, shorter are the ignition delays.

References

1 JAIN, S R , KRISHNA, P M M AND PAI VERNEKER, V R — Hypergolic ignition of various hydrazones with nitric acid, *J Spacecraft Rockets*, 1979, **16**, 69–73

2 RAJENDRAN, G AND JAIN, S R — Novel solid hypergolic fuels for hybrid propellants, *Fuel*, 1984, **63**, 709–712

3. JAIN, S R AND RAJENDRAN, G — Chemical aspects of the hypergolic preignition reactions of some hybrid hypergols, *Combust Flame*, 1987, **67**, 207–215

Thesis Abstract (Ph.D.)

The infinitely strong shock: towards an exact solution by Padarbinda Das.
Research supervisors: R. Narasimha and M. R. Ananthasayanam.
Department: Aerospace Engineering.

1. Introduction

Many problems in rarefied gas dynamics are governed by the nonlinear Boltzmann equation. The Boltzmann collision integrals, which are nonlinear and highly complex, present considerable difficulties in the solution of these problems. Few exact solutions exist, though the neighbouring field of linear transport theory is well studied.

The structure of a strong shock has a significance in kinetic theory similar to that of a flat-plate boundary layer in viscous flow theory—it shares many important features with a wide class of flows. In addition, it provides a simple test case for solving the nonlinear Boltzmann equation. In the present work, the structure of an infinitely strong (an infinite upstream Mach number) shock in gas of rigid spheres has been studied semi-analytically.

2. Main contributions

(i) Traditional polynomial expansions have failed to provide solutions for strong shocks. The Mott–Smith ansatz[1] provides solutions which are qualitatively acceptable, but are sensitive to the error (residual) criteria used along with the ansatz. There is no obvious way of improving the Mott–Smith solutions. Here, a novel rational approximation scheme to compute an exact solution to the infinitely strong shock has been presented.

(ii) Three successive approximate solutions have been computed in the above-mentioned scheme to obtain a density profile which is exact over most parts of the shock, and an exact value for the shock thickness at 6·7 times the downstream mean free path.

(iii) The scheme involves an expansion on the basis of 'Burnett functions', which consists of Sonine polynomials[2] and spherical harmonics[3]. Expressions, some of which are new, have been derived for the Boltzmann collision operators on this basis, and have been shown to possess high symmetry.

(iv) Computation of collision matrix elements has remained a difficult problem. Here the most efficient and reliable algorithms for computing these have been described at one place, and complete computer programs have been developed and listed. This technology overcomes a major obstacle to using polynomial expansions in kinetic theory.

(v) The relevant algebraic work has been carried out in the framework of a powerful irreducible tensor formalism[4] and Dirac notation[5]. The formalism had been employed earlier in kinetic theory, but its use in a highly nonlinear problem like the present one demonstrates for the first time its power in handling flows involving large departments from equilibrium.

(vi) The irreducible tensor formalism is a compact operational method of handling tensors of arbitrary ranks. Hence, it has great potential for application in continuum mechanics.

3. Formulation and solution

The Boltzmann equation[2] for the plane shock problem is an obvious notation as

$$\frac{\delta f}{\delta x}\,[v_x f] = J\,[f,f] \equiv G[f,f] - f\,L[f]. \tag{1}$$

Upstream and downstream, f approaches the respective Maxwellians F_1 ($= n_1\,\delta\,(v - u_1)$) and F_2.

The upstream molecular beam gradually attenuates across the shock, so f is given within the shock by

$$f(v,x) = -\,\nu_0(x)\,F_1 + h(v;x) \tag{2}$$

The form (2) of f implies that both sides of (1) have singular terms Equating the singular and non-singular parts separately, eqn (1) breaks down to

$$u_1 v_0' = - \nu_0 L[h] \ (u_1), \tag{3}$$

$$\nu_x \frac{\delta h}{\delta x} = \nu_0 \{G[F_1, h] + J[h, F_1]\} + J[h, h]. \tag{4}$$

The crucial step is to expand h in a series of polynomials, the Burnett functions $\psi^i(c)$ (where $c = \nu - u_2$) have been chosen for their great merit[4], around the fixed Maxwellian F_2

$$h(\nu_x x) = \nu_i(x) \ F_2(c) \ \psi^i(c) \equiv \nu_i(x) \ \phi^i \ (c) \tag{5}$$

A Galerkin-type procedure requires the expansions

$$\nu_x \phi^i = A_k^i \ \phi^k, \tag{6}$$

$$J[\phi^i, \phi^j] = J_k^{ij} \phi^k = [G_k^{ij} - L_k^{ij}] \ \phi^k, \tag{7}$$

and

$$F_i(c) = \delta_i \phi^i. \tag{8}$$

Using (5–8) in (3, 4) results in

$$\nu_0' = C_i \nu_0 \nu_i \tag{9}$$

$$A_k^i \ \nu_i' = B_k^i \ \nu_0 \ \nu_i + J_k^{ij} \ \nu_i \nu_j \qquad (i, j, k = 1, 2, \ ). \tag{10}$$

All the coefficients in (9, 10) are expressible in terms of the matrix elements A_k^i, $L[\phi^i]$, G_k^{ij} and L_k^{ij} Expressions have been derived for these matrix elements.

The solution orbits for (9, 10) must connect upstream and downstream equilibrium conditions. Such solutions are extremely difficult to compute. Successive approximate solutions to (9, 10) have been computed truncating the expansion (5) after one, four, and six terms

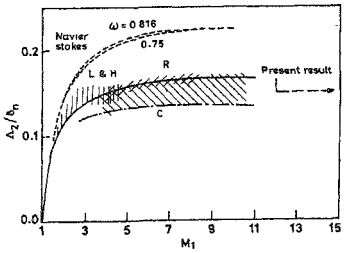

FIG 1 The present value of shock thickness marked on the plot given in Narasimha and Deshpande[6], ————, Mott-Smith minimum error solution of Ref 6; —— · ——, Mott-Smith ν_5^i moment values with $\omega = 0{\cdot}816$ ($\mu \sim T^\omega$). Hatched areas represent experimental values, (δ_n is shock thickness, Ω_2 is downstream mean free path)

The success of this work indicates that similar approaches might work for other nonlinear problems in rarefied gas dynamics

References

1 MOTT-SMITH, H M. *Phys Rev*, 1954, **82**, 885–892

2 CHAPMAN, S AND COWLING, T G *The mathematical theory of non-uniform gases*, 1939, Cambridge University Press

3 EDMONDS, A R *Angular momentum in quantum mechanics*, 1957, Princeton University Press

4 KUMAR, K *Ann Phys*, 1966, **37**, 113–141

5 MERZBACHER, E *Quantum mechanics*, 1961, Wiley

6 NARASIMHA, R AND DESHPANDE, S M *J Fluid Mech*, 1969, **36**, 555–570

Thesis Abstract (Ph.D.)

Some studies on structural dynamics of spacecraft systems by M. Sambasiva Rao.
Research supervisors: S. Durvasula and P. S. Nair.
Department: Aerospace Engineering.

1. Introduction

This work is concerned with some important aspects of structural dynamics of spacecraft and its subsystems These are broadly classified as free vibration data reduction, generation of dynamic models, free vibration studies on structural panels and equipment platforms and displacement excitation analysis.

It is shown that by the introduction of three modal parameters, namely, energy distribution, effective inertance and effective mass, the task of data reduction and interpretation of massive free vibration data output of typical finite element analysis of a large degree of freedom spacecraft structure is rendered very convenient and effective[1] The second parameter, namely, 'effective inertance', is a concept introduced perhaps for the first time in the present work in the context of matrix methods of structural analysis to derive significant advantages The 'energy distribution' indicates, within a mode, the relative contribution of various areas to the overall kinetic and strain energies Effective inertance gives information on individual modal contributions to the overall acceleration responses at different points in a structure subjected to a force excitation Effective mass represents the modal contributions to the total reaction force of a structure when excited by an acceleration input Application of these parameters in a spacecraft situation is illustrated with examples.

2. Equivalent dynamic models

The concept of effective mass is applied in obtaining 'equivalent dynamic models' of spacecraft structural systems/subsystems These models consist of simple physical elements like springs and beams and accurately represent the interface forces Their advantages over conventional mathematical models in analysis and testing are highlighted and their validity is illustrated through the example of a spacecraft Some of the practical problems associated with the physical simulation of these models in an actual dynamic test set-up are also addressed. Further, a systematic approach is outlined for developing 'low-order dynamic models' of spacecraft for use in coupled analysis with launch vehicle to obtain accurate loads at the interface and in important subsystems. A substructure method in which important subsystems are represented by equivalent dynamic models is suggested for this purpose during the development phase of a spacecraft project. The construction of such models and their usage in design parametric studies is also demonstrated through the example of Indian Remote Sensing satellite (Fig. 1)[2].

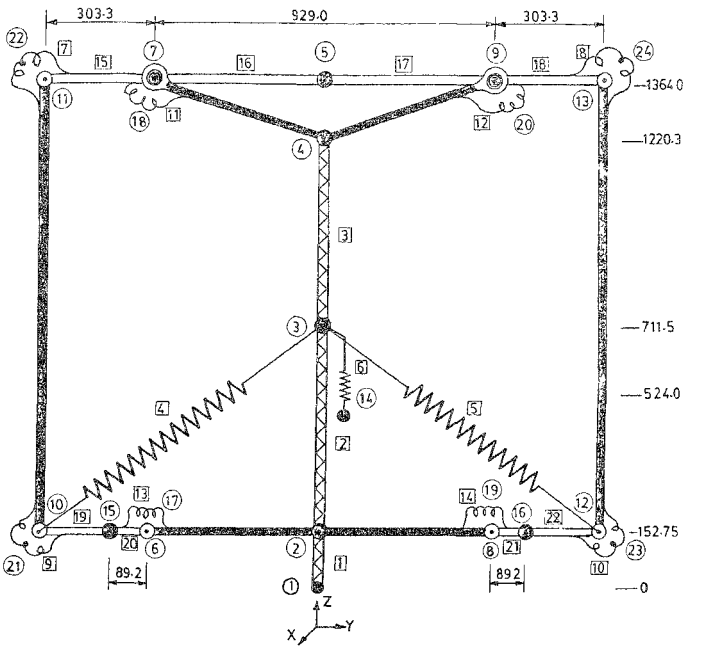

FIG 1a IRS low-order longitudinal dynamic model (all dimensions are in mm)

3. Free vibration of panels

A spacecraft consists of structural panels which provide shielding for sensitive electronic packages and equipment decks which carry electronic boxes, and both are designed to meet specific frequency constraints. The structural panels are generally stiffened using stiffeners to raise their frequencies. The effect

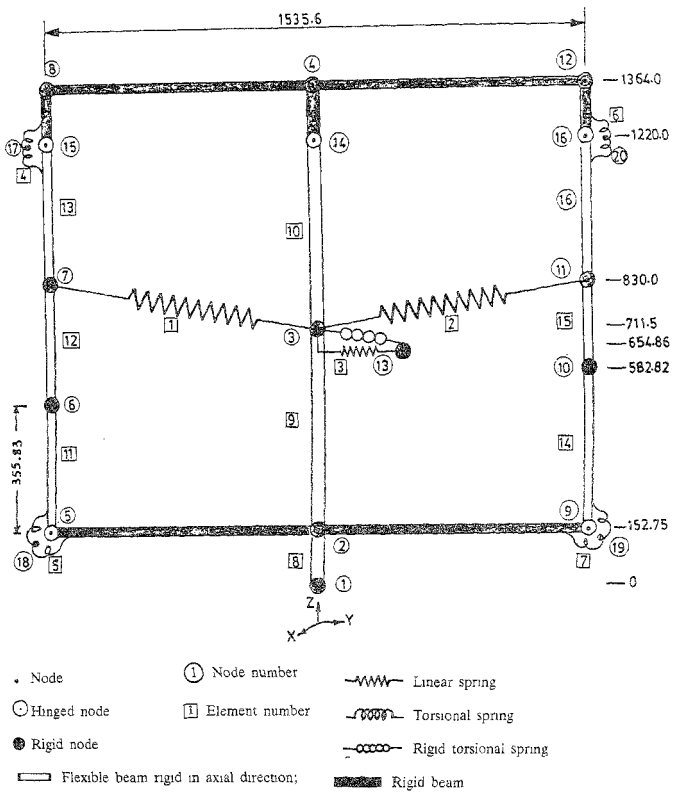

FIG 1b. IRS low-order lateral dynamic model (all dimensions are in mm)

of small gaps usually left between the stiffener end and boundary due to fabricational reasons in such panels is investigated with respect to their design efficiency and analysis problems for free vibration characteristics. It is found that in the case of clamped panels avoidance of this gap results in a significant jump in certain frequencies (Fig. 2)[3]. Through the example of a spacecraft equipment deck of honeycomb

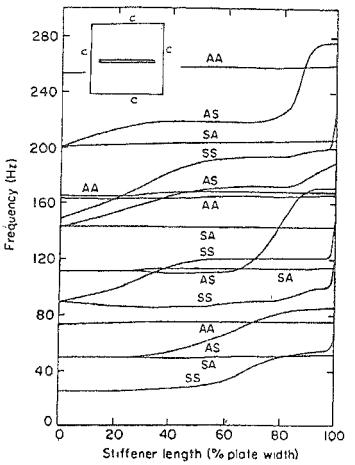

FIG 2 Variation of panel frequency with stiffener length (C Clamped)

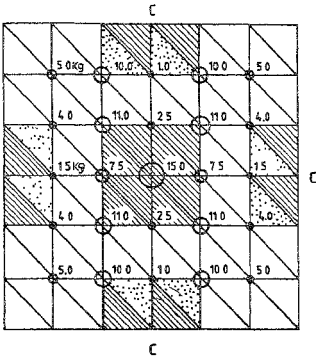

FIG 3a Design modification of honeycomb sandwich plate for frequency Elements with strain energy density more than average in fundamental mode are shown hatched Doublers are used in this area to increase the plate frequency From practical considerations elements shown dotted also can be stiffened

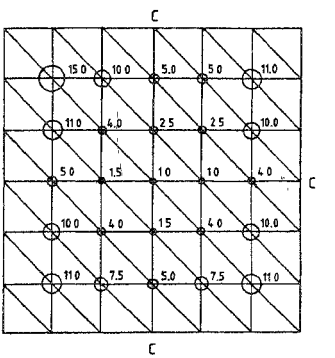

FIG 3b Modified mass distribution based on kinetic energy density for maximum fundamental frequency

sandwich construction, it is shown that the modal energy distribution can be used as effective guideline in improving its frequencies Kinetic energy distribution is employed as a basis for redistributing various packages on the deck and strain energy distribution is used to identify areas which can be stiffened by bonding doublers (Fig. 3)[4].

4. Displacement excitation analysis

The displacement excitation response analysis procedures, as implemented in SAP IV, ASKA and NASTRAN, are compared. This is done as no such information is available in literature on their relative efficiencies and because of the importance of displacement excitation analysis in a spacecraft case. It is found that ASKA results are in considerable error compared to other programs for the same number of modes included in the computations. It is shown that if mode acceleration, instead of the presently available mode displacement approach, is followed in ASKA, the results get significantly improved.

References

1 NAIR, P S, SAMBASIVA RAO, M. AND DURVASULA, S — Vibration data reduction for design, analysis and testing of spacecraft, *Proc FEICOM 85*, Bombay, 1985, pp 677–688

2 SAMBASIVA RAO, M., PRAKASH, B G AND PRABHU, M S S — Low order dynamic models of Indian Remote Sensing satellite, *Shock Vibr Bull*, 1985, **55**, 129–153

3 NAIR, P S AND RAO, M S — On vibration of plates with varying stiffener length, *J Sound Vibr.*, 1984, **95**, 19–29

4 SAMBASIVA RAO, M, NAIR, P S AND DURVASULA, S — Use of modal energy distribution in the design of honeycomb sandwich decks, *J Computers Struct*, 1988, **28**, 737–743

5 SAMBASIVA RAO, M — An evaluation of base-excitation response analysis using ASKA, *J Computers Struct*, 1986, **22**, 815–822

Thesis Abstract (Ph.D.)

Development and critical assessment of a new FLIC method for base flows by Sushil K. Saxena.
Research supervisors: R. Narasimha, S. M. Deshpande and T. S Prahlad (ISRO).
Department: Aerospace Engineering.

1. Introduction

The motivation for the present work stems from two complex base flow problems of relevance to satellite launch vehicles, namely, the flow about the base of a rocket body containing an exhaust jet and the aerodynamics of stage separation during the flight of a multistage rocket. The conventional FLIC (fluid in cell) has certain favourable features with regard to computation time, memory requirement and application of boundary conditions. It is however first-order accurate in space and time and therefore when applied to base flow problems produces results which though qualitatively correct are not quantitatively sufficiently accurate. Further, there is unacceptable smearing of shocks. The major contribution of the present work has been the development of a new FLIC (NFLIC) method which is second-order accurate in space but first-order accurate in time and still retains the favourable features of the conventional FLIC method. The new method is tested on a laminar base flow problem of a backward-facing step and compared with computations done by other higher order schemes.

2. Analysis

Complete details of analysis are available elsewhere[1,2]. Here only the essential details are presented. The present work has resulted in the finding that eigenvalues of the Jacobian matrices for the FLIC convection terms are of the same sign, they are either all positive or all negative depending upon the sign of the velocity components. The flux splitting of convection-phase equations, which are Euler equations without pressure terms, therefore, turn out to be very simple compared to the flux splitting in the case of full Euler equations where the eigenvalues of the Jacobians of flux vector can be of mixed sign. These split fluxes are then used in a second-order accuracy in space in the convection phase. Phase I difference operator and the sequence of operators remains the same as in the case of conventional FLIC.

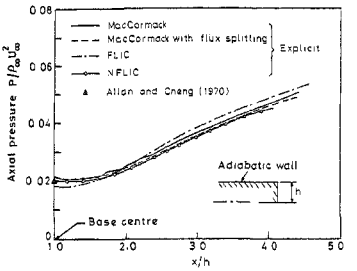

FIG 1 Laminar flow past backward-facing step ($M_\infty = 3.0$, $Re_h = 400$)

$$U^{n+1} = O_{II}\,(\Delta t)\; O_I\,(\Delta t)\; U^n$$

where O_I is the difference operator in the case of Phase I and O_{II} the difference operator for Phase II In the case of NFLIC, the operators O_I and O_{II} are both second-order accurate in space but first-order accurate in time The above sequence of operators provides overall second-order accuracy in space but first-order accuracy in time for the new method

The efficiency of FLIC has been improved by employing convergence acceleration devices which include grid sequencing and local time stepping A box-type grid distribution has been employed to discretize the solution domain in the case of low Reynolds number flows, while an exponentially stretched grid is recommended for high Reynolds number cases to keep the grid point requirements low. Finer grid has been used in the boundary layer and at viscous region near the base corner

3. Results and discussion

Detailed results from FLIC and NFLIC obtained on various base flow problems are presented in the thesis Here only some representative results from NFLIC on a laminar base flow problem of a backward-facing step are presented and compared with the results from other higher order schemes which include MacCormack's explicit scheme employing operator splitting with and without flux vector splitting and an

Table I
Comparison between different numerical methods in terms of operation count and memory requirement

Method	*Operation count (Million instructions per time step per grid point)*	*Core memory for 1130 grid points*
MacCormack's explicit scheme	0 0081	43 K (60-bit word)
MacCormack's explicit scheme with flux vector splitting	0 017	45·5 K
Classical FLIC	0 0050	39 K
New FLIC	0 0075	39 K
Unfactored implicit upwind scheme	0 0730	61 K

unfactored upwind implicit scheme Figure 1 presents the axial pressure distribution and indicates favourable comparison of NFLIC with other second-order accurate methods in terms of accuracy Although not presented here, similar good comparison is obtained for cross total pressure variation and contour plots of Mach number, streamline and velocity vector Table I presents the comparison of NFLIC with other second-order accurate methods mentioned above in terms of operation count and memory requirement It is clear from the table that the new method has certain edge in this regard compared to the explicit methods based on the flux vector splitting of the full Euler equations

4. Conclusion

A new FLIC method (NFLIC) within the framework of finite volume approach has been successfully developed which is upwind and second-order accurate in space and still retains various favourable features of the conventional FLIC method It has been critically assessed with regard to accuracy, operation count and memory requirement by testing it on a laminar base flow problem of a backward-facing step and comparing with the results from other higher order accurate schemes It is shown to have certain edge in terms of operation count and memory requirement over other explicit methods based on the flux vector splitting of the full Euler equations The efficiency of FLIC has been improved by employing grid sequencing and local time stepping by a factor of six

References

1 SAXENA, S K , DESHPANDE, S M AND PRAHLAD, T S — An improved FLIC for supersonic base flow, *AIAA paper 87-1148-CP, 8th CFD Conf* , Honolulu, Hawaii, June 9–11, 1987

2 SAXENA, S K , DESHPANDE, S M NARASIMHA, R AND PRAHLAD, T S — Numerical simulation of base flow, *Proc Second Asian Congr Fluid Mech* , Beijing, China, Oct 1983

Thesis Abstract (Ph.D.)

Steady compressible plane flow of cohesionless granular materials in hoppers and bunkers by J. Ravi Prakash.
Research supervisor: K. Kesava Rao.
Department: Chemical Engineering.

1. Introduction

The slow flow of granular materials is commonly described by frictional theories which are similar to those used in plasticity and soil mechanics[1,2] These theories have been applied to incompressible flow through hoppers[3, 4] However, observations of density profiles indicate that there are significant changes in certain parts of the flow field[5] Therefore, it is desirable to examine the compressible flow of granular materials from a theoretical viewpoint The present work examines the steady, plane, compressible flow of cohesionless granular materials through a hopper and a bunker with a view to predict the stress, velocity and density fields, and to compute discharge rates A continuum model based on the critical state theory of soil mechanics[6] is used for this purpose

2. Results

The one-dimensional situation of a hopper with smooth walls and gravity directed radially towards its apex is first considered. Results are found to be relatively insensitive to the shape of the yield locus, the location of the upper traction-free surface, and the density specified on this surface. This insensitivity arises from the existence of asymptotic stress and density fields to which the solution tends to converge on moving down the hopper Approximate expressions are derived for the asymptotic fields, and discharge rates estimated using these expressions are within 13% of the exact (numerical) values Finally, it is shown that the assumption of incompressibility leads to discharge rates which are significantly higher than those obtained by the incorporation of density variation.

The two-dimensional situation of a mass-flow bunker is the second problem considered here The bin-hopper transition region is idealized as a shock across which all the variables change discontinuously Comparison with the work of Michalowski[7] shows that his experimentally determined rupture layer lies between the prediction of the present theory and that of Michalowski[7] However, it resembles the latter more closely The conventional condition involving a traction-free surface at the hopper exit is abandoned in favour of an exit shock below which the material falls vertically with zero frictional stress The basic equations, which are not classifiable under any of the standard types, require excessive computational time This problem is alleviated by the introduction of the Mohr-Coulomb approximation (MCA). The stress, density, and velocity profiles obtained by integration of the MCA converge to asymptotic fields on moving down the hopper Expressions for the fields are derived by a perturbation method Computational difficulties are encountered for bunkers with wall angles $\theta_W \geq 15^0$, these are overcome by altering the initial conditions. Predicted discharge rates lie significantly below the measured values of Nguyen *et al*[8], ranging from 38% at $\theta_W = 15^0$ to 59% at $\theta_W = 32^0$ This poor prediction appears to be largely due to the exit condition used here. Paradoxically, incompressible discharge rates lie closer to the measured values An approximate semi-analytical expression for the discharge rate is obtained, which predicts values within 9% of the exact (numerical) ones in the compressible case, and 11% in the incompressible case. The approximate analysis also suggests that inclusion of density variation decreases the discharge rate This is borne out by the numerical results

References

1 NEDDERMAN, R M , TUZUN, U , SAVAGE, S B AND HOULSBY, G T — The flow of granular materials – I, *Chem Engng Sci* , 1982, **37**, 1597–1609

2 JACKSON, R — Some mathematical and physical aspects of continuum models for the motion of granular materials In *Theory of dispersed multiphase flow* (ed Meyer, R E), 1983, pp 291–337, Academic Press

3 BRENNEN, C AND PEARCE, J C — Granular material flow in two-dimensional hoppers, *Trans ASME, J Appl Mech* , 1978, **45**, 43–50

4. KAZA, K. R. AND JACKSON, R — The rate of discharge of coarse granular material from a wedge-shaped mass flow hopper, *Powder Technol* , 1982, **33**, 223–237

5. FICKIE, K E , MEHRABI, R AND JACKSON, R — Density variations in a granular material flowing from a wedge-shaped hopper, *AIChE J*, 1989, **35**, 853–855

6 SCHOFIELD, A. N AND WROTH, C P — *Critical state soil mechanics*, 1968, McGraw-Hill

7 MICHALOWSKI, R L — Flow of granular media through a plane parallel/converging bunker, *Chem Engng Sci* , 1987, **42**, 2587–2596

8 NGUYEN, T V , BRENNEN, C E. AND SABERSKY, R H. — Funnel flow in hoppers, *Trans ASME, J Appl Mech* ,1980, **47**, 729–735

Thesis Abstract (Ph.D.)

Studies on two-dimensional separation bubbles and associated unsteady pressure fields

by H. S. Govinda Ram.
Research supervisor: V H. Arakeri.
Department: Civil Engineering.

1. Introduction

Pressure fluctuations are of common occurrence in unsteady fluid flows A need to measure these has been a long-felt need with reference to aerodynamic applications like jet noise, aircraft cabin noise, etc. Similarly, knowledge of the pressure fluctuation characteristics is an essential ingredient of predicting and understanding of 'sonar' self-noise in underwater applications[1]. The possible role of pressure fluctuations

in the problem of cavitation inception has been realized for some time, but, perhaps the first systematic study in this direction has been due to Arndt and Ippen[2] These studies were limited to wall-bounded turbulent flows. Subsequent studies by Araken[3] and Huang and Hannan[4] have shown that the role of turbulent pressure fluctuations can be even more dramatic for certain class of flows like separating shear layers. Substantially stronger-magnitude pressure fluctuation levels have been measured in certain regions of such flows than those existing in attached fully developed turbulent boundary layers Recently, Katz[5] has carried out extensive pressure fluctuation measurements in flows with laminar separation and subsequent turbulent reattachment However, one of the questions which remained unanswered was whether the fluctuation levels could be even higher in the developing shear layer away from the surface than those measured at the surface itself It is of interest to note that Katz[5] measured surface rms pressure fluctuation levels as high as 19 per cent of the dynamic head on a blunt cylindrical nose model A natural question which arises is whether there is an upper limit for the rms pressure fluctuation levels either in the flow or at the surface This is relevant from the point of view that cavitation inception index for flow past a sharp-edged disk does not seem to show an upper bound with increase in Reynolds number[6]

In the past, basically, two types of pressure fluctuation measurements in turbulent flows have been attempted, namely, surface and within the flow The former are much more numerous than the latter, the majority of the former and to the best of our knowledge all the latter have been carried out using wind tunnel facility rather than water tunnels. Some specific references directly relevant to the present studies are available in two review articles by Willmarth[7] and George *et al*[8] The present study is aimed at fulfilling certain gaps in the measurement of pressure fluctuations in one class of flows where the boundary layer at separation from a forebody is laminar and the flow reattaches on a splitter plate turbulently In particular, attempts for the first time have been made to measure both the surface-pressure fluctuations and pressure fluctuations within the flow in the region of separation and reattachment For pressure fluctuation measurements within the flow, a 'probe microphone' was constructed along similar lines of a probe used by Arndt and Nilsen[9]

2. Experimental methods

The facility used for the present experimental study is a suction-type low-speed wind tunnel The cross-sectional area of the test section is 610 × 610 mm and the total length is 2100 mm The tunnel contraction ratio is 9 : 1. To provide as quiet an environment as possible for pressure fluctuation measurements, the transmission of the diffuser vibration was minimized by providing a flexible attachment between the diffuser and the test section. Different nose model shapes were used in the present study The first set of models selected were isosceles two-dimensional triangular cylinders The second set of models, also two-dimensional, consisted of 1 . 2 ratio elliptical nose, semicircular nose and right-angle corner blunt edge plate. The two-dimensional models were mounted with perspex splitter plate, spanning the test section In addition to the two-dimensional models mentioned, two axisymmetric blunt cylindrical models were also used in the present study The surface static pressure fluctuations were measured with B & K condenser microphone mounted close to the surface of the splitter plate The output of the microphone was fed into a B & K cathode follower built-in preamplifier, and finally to a measuring amplifier/frequency analyzer Measurement of pressure fluctuations within the flow was made with a probe very similar to the one used by Arndt and Nilsen[9] The resonance peak was reduced by placing glass wool as damping material

3. Results and discussion

Extensive investigative runs were made to assess the background noise levels of the facility, frequency contents of the unsteady pressure and velocity fields and the two dimensionality of the flow field in the central region of the splitter plate In addition to the measurements to be presented, the reattachment distance for the various models was quantitatively estimated using several techniques. The distance x along the plate is non-dimensionalized with respect to the mean reattachment length X_R. In all the cases, the mean pressure coefficient remains nearly constant up to about $x/X_R = 0{\cdot}4$. The base pressure coefficient C_{pb} varies significantly with 2Θ values of a triangular nose A reasonably good collapse is found with modified pressure coefficient C_p^* defined as $C_p^* = (C_p - C_{pb})/(1 - C_{pb})$, where C_p is the pressure coefficient along the plate

The maximum normalized levels of surface pressure fluctuations depend strongly on 2Θ values, and occur at $x/X_R = 0{\cdot}9$ But for the shear layer pressure fluctuations it occurs at $x/X_R = 0{\cdot}75$

4. Conclusions

The primary conclusions from the present experimental study are

1 The maximum normalized rms surface pressure fluctuation levels showed a dependence on the 2Θ value of the triangular-shaped forebodies which varied from about 10 per cent of the dynamic head for $2\Theta = 30$ degree model to 15 per cent for $2\Theta = 180$ degree model For the other 2Θ angle geometries the maximum levels were between the two extremes noted

2 There appears to be a correlation between the maximum normalized value of the rms surface pressure fluctuation levels and the base pressure coefficient For the two-dimensional forebodies used presently, the ratio $C_{p'max}/(-C_{pb})$ has a value of about 0 23.

3 Except for the $2\Theta = 180$ degree model, for all the other triangular nose models, the maximum rms pressure fluctuation levels in the shear layer are almost equal to the maximum surface rms pressure fluctuation levels This finding has come as somewhat of a surprise For the blunt $2\Theta = 180$ degree model, the maximum pressure fluctuation level in the shear layer is larger by about 4 per cent of the dynamic head.

4 In the overall context, the probe microphone response has been found to be quite satisfactory and could be developed into a reliable instrument for measurement of pressure fluctuation levels within the flow.

References

1. BLAKE, W K — *Mechanics of flow-induced sound and vibration*, 1986, Academic Press

2 ARNDT, R E A AND IPPEN, A T — Rough surface effects on cavitation inception, *ASME J Basic Engng*, 1968, **90**, 249–261

3 ARAKERI, V H — A note on the transition observations on an axisymmetric body and some related fluctuating wall pressure measurements, *ASME J Fluids Engng*, 1975, **97**, 82–87

4 HUANG, T T AND HANNAN, D. E — *Pressure fluctuations in the region of flow transition*, Rep No 4723, Naval Ship R and D Centre, Washington, DC, Dec. 1975

5 KATZ, J — *Cavitation inception in separated flows*, Ph.D Dissertation, California Institute of Technology, 1981

6 KERMEEN, R W AND PARKIN, B R — *Incipient cavitation and wake flow behind sharp edge disks*, Rep No 85–4, Hydrodynamic Laboratory Report, California Institute of Technology, Aug 1957

7 WILLMARTH, W W — Pressure fluctuations beneath a turbulent boundary layer, *A Rev Fluid Mech*, 1975, **7**, 13–38

8 GEORGE, W K, BENTHER, P D AND ARNDT, R E A — Pressure spectra in turbulent free shear flows, *J Fluid Mech*, 1984, **148**, 155–191

9 ARNDT, R E A AND NILSEN, A. W. — *On the measurement of fluctuating pressure in the mixing zone of a round jet*, ASME Fluid Engineering Division, Paper No 71-FE-31, 1971

Thesis Abstract (Ph.D.)

Sub-optimal control *via* lower order generalised aggregated models by P. S Satyanarayana.

Research supervisor: M. R. Chidambara.
Department: Computer Science and Automation.

1. Introduction

One of the most widely studied problems in the field of modern control theory is the 'optimal linear

regulator problem' The 'curse of dimensions', computational complexity, memory requirements of the available digital computer and the need of an observer to make all the state variables available for feedback pose problems in deriving and implementing an optimal control law In such circumstances, the design engineer is forced to seek easily implementable sub-optimal solutions. One way of getting such solutions is by the use of a reduced order model This work provides a novel method of achieving the goal.

2. Contribution of the thesis

Majority of the available model reduction techniques deal with open-loop behaviour of the model and the original system Even when they can be used for sub-optimal control, problem of implementation remains unsolved Further, an error between the output responses of the original system and the model always does exist due to the absence of certain modes (equal to the difference between the orders) of the original system An improvement in the situation can be obtained by using the idea of Chidambara and Schainker[1] to excite the model by an additional input proportional to the output response error thereby forcing the model to contain all the modes of the original system Because of its similarity with the aggregated model of Aoki[2] and the observer of Luenberger[3] the resultant model is called a 'generalised aggregated model' (GAM). The work reported is a refinement of this novel idea and makes the framework of 'generalised aggregation' more meaningful and powerful in the control of large-scale systems.

In this work, GAM is made directly compatible for sub-optimal design for multi input–multi output (MIMO) systems by forcing the weighting matrix of the output response error to be the product of the control distribution matrix of the GAM and α, a matrix of feedback gains for the original system. GAM is constructed by using dominant eigenvalues of the 'closed loop original system with output feedback, $-\alpha$', thus not requiring a knowledge of the original system (open loop) eigenvalues The power of the approach lies in the proper choice of α, which is dependent on the subjective judgement of the designer. The aggregation matrix is unique for a chosen error-weighting matrix and is obtained as the unique solution to a linear matrix equation The output matrix of the GAM is chosen to given minimum 'integral squared-impulse response error' (IS-IRE) subject to the condition of zero 'steady-state step-response error' (SS-SRE)

When GAM is used for sub-optimal design, it is found that the choice of α that gives an absolute minimum IS-IRE does not necessarily result in absolute minimum performance degradation (PD), and *vice versa*. Thus, there exists a trade-off between IS-IRE and PD which requires the subjective judgement of the designer

Whereas GAM can be directly used to solve an output regulator problem, the state regulator problem is solved using a 'dis-aggregation' procedure Unlike in other sub-optimal controls, for the sub-optimal control presented in this work, it is shown that the closed-loop stability of the original system is always guaranteed. It is established that the poles of the closed-loop original system when GAM-based control law is used are those eigenvalues of the closed-loop system with output feedback matrix $-\alpha$, not used in constructing GAM and (optimal) closed-loop poles of GAM This unique feature of the proposed GAM provides considerable flexibility in deciding the order of the GAM depending on the allowable tolerance on PD Numerical examples are given to illustrate the utility and superiority of the proposed technique.

Another interesting use of GAM framework is in deriving stabilising control policies (pole placement). Solution for this problem is straightforward when using GAM and an iterative procedure for the same is outlined in the work In general, the MIMO pole placement problem can be converted into a problem of solving a set of underdetermined equations by using the GAM technique When GAM is intended for solving the pole-placement problem, the α-matrix and the output matrix of GAM can be chosen at will, without bothering about IS-IRE and optimisation procedure

One of the most important applications of the GAM proposed in this work is in the design of systems for a desired transient response (problem of partial pole placement). Solution for such a problem, using conventional pole-placement methods requires, for feedback, a linear combination of either all the state variables or a subset of the state variables. In the latter case, a transformation of the system to its decoupled form is required In either case, it is necessary to build an observer to make all the state variables individually available for implementing the control law It has been shown in this work that it

is possible to shift only a subset of the poles of the system (say m poles of the nth order system) by the construction of an mth order GAM and the solution of an nth order pole-placement problem GAM, viewed as an observer, then eliminates the need of a full-order observer in the conventional sense requiring only an observer of order equal to the number of eigenvalues of the original system to be changed to be constructed.

Finally, the utility of GAM in sensitivity-reduced design of linear regulators has been brought out The procedure does not require the generation and feedback of either the state variables or the trajectory sensitivity vector of the original system The design depends on the choice of a solar parameter β which in turn depends on the allowable performance degradation

In all cases, implementation of the control law is done using 'measurement variables' of GAM alone and thus no observer is required

References

1	CHIDAMBARA, M R AND SCHAINKER, R B	Lower order generalised aggregated model and sub-optimal control, *IEEE Trans* , 1971, AC–16, 175–180
2	AOKI, M	Control of large-scale dynamic systems by aggregation, *IEEE Trans* , 1968, AC-13, 246–253
3	LUENBERGER, D G	Observing the state of a linear system, *IEEE Trans* , 1964, MIL-8, 74-80

Thesis Abstract (Ph.D)

Development of quaternary circuits using CMOS quaternary multiplexers as building blocks by G. Krishnan.
Research supervisor: A. P. Shivaprasad.
Department: Electrical Communication Engineering.

1. Introduction

The reduction in the size of an integrated circuit has been one of the important hardware requirements in LSI/VLSI design This can be achieved by (i) the reduction in the size of components using sophisticated technology which has an ultimate limit due to the problems associated with control, handling, etc , and (ii) the reduction in the number of node points, interconnections on chip wiring and interchip wiring (*i e.*, number of pins), which requires that the information carried by each connection or line be increased But so long as the logic used for the digital circuit design is binary, there is an ultimate limit with regard to miniaturization due to the limited functional density of the binary logic. Therefore, there is a necessity to bring up a new logic family which can provide higher functional density and this has led to the development of multiple-valued logic as an alternative to binary

2. Multivalued logic (MVL)

Any radix more than two is called multiple-valued radix and the associated logic as the multiple-valued logic or simply multivalued logic (MVL). As MVL can carry more information on each line, it provides more functional density (*i e* , elementary functions/mm^2) and less number of pins in a chip Hence, a systematic development of MVL is required As on today, no MVL has reached a stage of perfection to compete with binary logic in digital design and replace it. But, quaternary appears to be the best choice for immediate acceptance since radix four is the next higher radix to binary with a power of two Hence, this work deals mainly with the quaternary logic circuits and systems.

3. Quaternary logic circuits and systems

The problems attempted in this direction are (a) development of quaternary algebra, (b) formulation of quaternary functions and simplification techniques, (c) design and development of universal logic modules

(ULM) and their standardization, and (d) design and development of elementary blocks such as adders, multipliers, analog-to-quaternary converters (AQCS) and quaternary-to-analog converters (QACS), etc., using quaternary universal logic modules.

3 1. *The gate-level design*

Quaternary algebra, function formulation, simplifications and realizations relating to the gate level of design complexity have been studied. Various CMOS logic gates suitable for the development of quaternary logic have been identified and performances of the gates assessed.

3 2. *MSI-level design*

As the gate level of design requires involved methodology and results in complicated circuitry, a quaternary multiplexer as an MSI building block has been examined to assess its suitability in designing the quaternary logic. Three different configurations of quaternary multiplexers have been proposed for developing quaternary circuits under the MSI level of design complexity. Hardware configurations and simulation models have been developed and methodologies proposed for function formulation, simplification and realization using quaternary multiplexers as the basic building modules A new mapping technique has been explicitly brought out for quaternary function simplification Using this methodology important quaternary combinational circuits such as adders, subtractors, multipliers, etc , have been designed and developed Algorithms are proposed for quaternary-coded addition and subtraction. Also, some useful configurations for analog-to-quaternary interface and instrumentation purposes have been proposed. It has been shown that the quaternary CMOS multiplexers developed serve as efficient building blocks in the realization of quaternary digital circuits/systems.

4. Conclusions

In all these investigations, the performance of quaternary systems has been compared with the equivalent binary systems, and both merits and demerits have been brought out highlighting the use of quaternary logic as an alternative to binary and the importance of quaternary MUX as a universal logic module in the design and development of quaternary systems[1-3].

References

1. Smith, K C — The prospects for multivalued logic. A technology and applications view, *IEEE Trans*, 1981, **C-30**, 619–634.

2 McCluskey, E J — A discussion of multiple valued logic circuits, *Proc Int Symp Multiple Valued Logic*, 1982, pp 200–205

3. Hurst, S L — Multiple-valued logic—its status and its future, *IEEE Trans*, 1984, **C-33**, 1160–1179

Thesis Abstract (Ph.D.)

Study of power system response to cyclic loads. Modelling—simulation-controller design by K. Raghavendra Rao.
Research supervisor: Lawrence Jenkins.
Department: Electrical Engineering.

1. Introduction

In addition to random variations in load (termed as disturbance) to which a power system is normally subjected, there are cyclic loads which have a periodic variation. Typical examples are the loads of nuclear reactors and steel plants where both the active and reactive power demands vary periodically. The presence of such large cyclic loads may result in undesirable power oscillations over the transmission lines supplying them and also result in large voltage dips, causing problems to consumers in the vicinity of such loads[1].

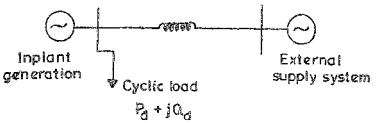

FIG 1 Two-machine system

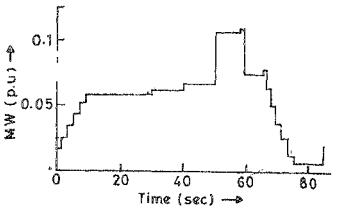

FIG 2 Load wave form active power

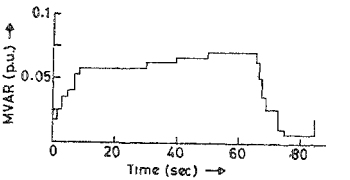

FIG 3 Load wave form reactive power

Further, large harmonic oscillations may be set up in the system itself as a result of some resonant modes in the system being close in frequency to either the fundamental or one of the harmonics of the cyclic load

2. System investigated

The proposed Vijayanagar Steel Plant (near Hospet in South India) is considered for the purpose of the study. To reduce the impact of the cyclic load on the power system and also to meet the essential loads when the external supply system fails, an inplant generation is necessary. The power system supplying such a load can be approximated by a two-machine system (Fig 1). Figures 2 and 3 show the variation of the active and reactive power demands of the cyclic load Both linear (suitable for small disturbances) and nonlinear models (suitable for large disturbances) are developed for the purposes of investigation.

3. A new technique for steady-state response of a power system due to cyclic load

The technique uses the method of harmonic analysis for determining the steady-state response to cyclic load. The load cycle is resolved into harmonic components and the system response to each one of the harmonic components is obtained by solving a set of linear algebraic matrix equations The total system response is obtained by applying the principle of superposition This method of analysis gives results of acceptable accuracy However, this technique is suitable for only linear systems

4. Multi time scale analysis

Classical methods of long time-simulation studies on a digital computer (as in the case of power system response to cyclic load) is prohibitively costly, as the period of simulation extends over a few minutes A two-time scale-simulation technique is developed and applied for such studies[2] Techniques suitable for both linear and nonlinear systems are presented. In the case of linear systems, the system model in the state space form is decoupled into two lower order subsystems, one group consisting of fast variables and the other of slow variables. These groups of state variables are simulated with different time steps. The subsystem responses are combined to get the total system response[5] This technique when applied for the simulation of cyclic load results in a 50 per cent reduction in computer time

The above decoupling technique cannot be applied for nonlinear systems But, if the coupling between the slow and fast subsystems is weak, such a property can be exploited for two-time scale simulation.

Using this technique, the power system response to large cyclic load (nonlinear model) is simulated and the saving in computer time by this approach is about 63 per cent.

5. Design of controller

Even though considerable research work has been done in the area of system optimization over the past two decades, most of the applications are limited to lower order systems In the case of higher order ill-conditioned systems the design of an optimal controller requires large computer time, in view of the slow convergence that arises due to the presence of both slow and fast modes The singular perturbation technique, when applied for the design of the controller, permits the regulator design to be decomposed into the design of two lower order subsystems, each being designed independently[1-6] This technique has been applied for the design of controller for a power plant supplying the cyclic load of a steel plant[5] The performance of such a regulator is compared with other types of regulators both in cost (computer time) and performance This technique of controller design is found to be more simple in design, requires less computer time and has almost the same performance index as that obtained by the classical methods

6. Conclusions

The response of a power system is basically characterized by the response characteristics of prime movers in the power plant when the period of study extends over a few minutes as in the case of cyclic load of a steel plant, the slow subsystems of the power plant such as boiler in a thermal power plant and surge tank in a hydro plant As they play a significant role, their dynamics should be incorporated in the power system model[6] For small disturbances created by the cyclic load the inplant generation follows more closely the change in demand But for large disturbances the major portion of the changing demand is supplied by the external supply system In both the cases, the deviation in frequency and voltage at the load bus are well within the permissible limits Singular perturbation technique provides simple and efficient methods for multi time scale simulation and controller design for higher order ill-conditioned systems

References

1 PINNELLO, J A AND VAN NESS, J E — Dynamic response of a large power system to a cyclic load produced by a nuclear accelerator, *IEEE Trans* , 1971, **PAS-90**, 1856–1862

2 RAGHAVENDRA RAO, K , JENKINS, L PARTHASARATHY, K AND BALASUBRAMANYAM, R — Multi-time scale analysis applied to long-time simulation of power systems, *Elec Pwr Energy Systems*, UK, 1985, **7**(1), 7–13

3 WINKELMAN, J R , CHOW, J H ALLEMONG, J J AND KOKOTOVIC, P V — Multi-time-scale analysis of a power system, *Automatica*, 1980, **16**, 35–43

4 SANNUTI, P AND KOKOTOVIC, P V — Near-optimum design of linear systems by a singular perturbation method, *IEEE Trans* , 1969, **AC-14**, 15–22

5 RAGHAVENDRA RAO, K AND JENKINS, L — Design of a near optimum regulator for a power plant, *Elect Mach Pwr Systems*, 1985, **10**, 1–14

6 YOUNG, C C. — Equipment and system modeling for large-scale stability studies. *IEEE Trans* , 1972, **PAS-91**, 99–109

Thesis Abstract (Ph.D.)

Lightning impulse breakdown behaviour of non-uniform field gaps in binary and ternary gas mixtures containing SF_6 at elevated pressures by D. Raghavender.
Research supervisor: M. S. Naidu.
Department: High Voltage Engineering.

1. Introduction

With increasing number of applications of sulphur hexafluoride (SF_6) gas in compact substations, switching

equipment, cables and other high-voltage apparatus, a complete knowledge of all aspects of its electrical breakdown behaviour has become essential. SF_6 gas is still expensive compared to other commonly used gaseous dielectrics and is very sensitive to local field enhancements which are inevitable in engineering applications because of the electrode surface protrusions and the presence of free-conducting particles. In the most commonly used pressure range, SF_6 gas retains only one half of its potential dielectric strength for practical electrode finishes[1,2].

In view of these problems in SF_6 gas-insulated equipment, investigations were carried out to obtain information on: (a) the physical processes that can influence the breakdown mechanisms, and (b) to develop an alternative gas/gas mixture to SF_6 which would meet all the requirements of a practical system (gas-insulated system) at moderate cost.

Gases and gas mixtures studied include N_2, SF_6, SF_6/N_2, SF_6/CO_2, $SF_6/CCl_2F_2/N_2$ and $SF_6/CCl_2F_2/CO_2$ with their pressures varying from 1 to 5 bars.

2. Experimental apparatus and procedure

Lightning impulse (1·2/50Ms) breakdown tests (up to 300 kV) have been carried out using a Marx-type, 10-stage impulse voltage generator of 500 kV rating. A cylindrical high-pressure chamber made of mild steel having a volume of 0·12m^3 and fitted with a high-voltage bushing was used. The electrode arrangement comprises various hemispherical-capped stainless steel rods of 0·1 (sharp needle), 0·8, 1·5, 3·0, 5·0 and 10·0 mm and a 230-mm dia plane electrode of Rogowskiprofile. The gap distances between electrodes varied from 5 to 80 mm (in some cases up to 100 mm) and were measured to an accuracy of better than ± 0·1%. Gases (SF_6, CCl_2F_2, N_2 and CO_2) of cylinder-grade purity (99·5%) were used and their mixtures prepared using the method of partial pressures to an accuracy of ± 0·2%. The 50% flashover voltages (V_{50}) have been measured using statistical methods such as step-by-step method and Bakken's method[3]. The values obtained by both the methods were in very good agreement (± 3%). These variations, however, do not indicate any uncertainty in V_{50}, and during the study, V_{50} could always be reproduced to within ± 2%. From the known gas content in the mixtures and from the measured breakdown voltages (V_{50}) a cost/benefit analysis has been carried out for the various binary and ternary gas mixtures investigated.

3. Results and discussion

3.1 *Breakdown in N_2 and 1% SF_6/99% N_2 mixtures under varying field non-uniformity*

A striking feature of the results obtained under lightning impulse (1·2/50 Ms) voltage conditions, in N_2 and 1% SF_6/99%N_2 mixtures using different rod–plane geometries (rod dia 0·1, 0·8, 1·5, 3·0, 5·0 and 10·0 mm) is that the V_{50}–rod diameter characteristics show minima in their V_{50} values at all gap spacings (5 to 80 mm) and gas pressures (1 to 5 bar). These minima (V_{50} min) do not appear to occur at any fixed value of rod diameter, but vary depending on the gas pressure and the gap spacing. The significance of V_{50} minimum in breakdown characteristics implies that for a given gap length a safe voltage level exists below which no breakdown can occur irrespective of the rod diameter and the gas pressure.

3.2 *Breakdown in binary (SF_6/N_2) and ternary mixtures ($SF_6/CCl_2F_2/N_2$ and $SF_6/CCl_2F_2/CO_2$)*

The present results indicate that in non-uniform field gaps pure N_2 is extremely sensitive to the presence of small quantities of SF_6. An increase in the positive breakdown voltage by as much as 70 to 100% was observed for SF_6/N_2 mixtures (0·1 to 20% SF_6 in N_2) at low pressures of about 0·1 MPa (1 bar) when the gap is 40 mm. This increase is more pronounced at gaps (740 mm) when the applied voltage is of negative polarity.

3.3 *Cost/benefit analysis*

A comprehensive study of the dielectric strength and costs of $SF_6/CCl_2F_2/N_2$ mixtures in comparison with expensive perfluorocarbons (2-C_4F_8, *n*-C_4F_{10} and C-C_4F_8)-based mixtures (SF_6/N_2/PFC), and pure SF_6(4) is shown in Fig. 1. From this it is seen that 1% SF_6/39% CCl_2F_2/60% N_2 and 20% SF_6/20% CCl_2F_2/60%N_2 mixtures contribute to the cost ratio by only about 0·12 and 0·27, respectively, at the same time

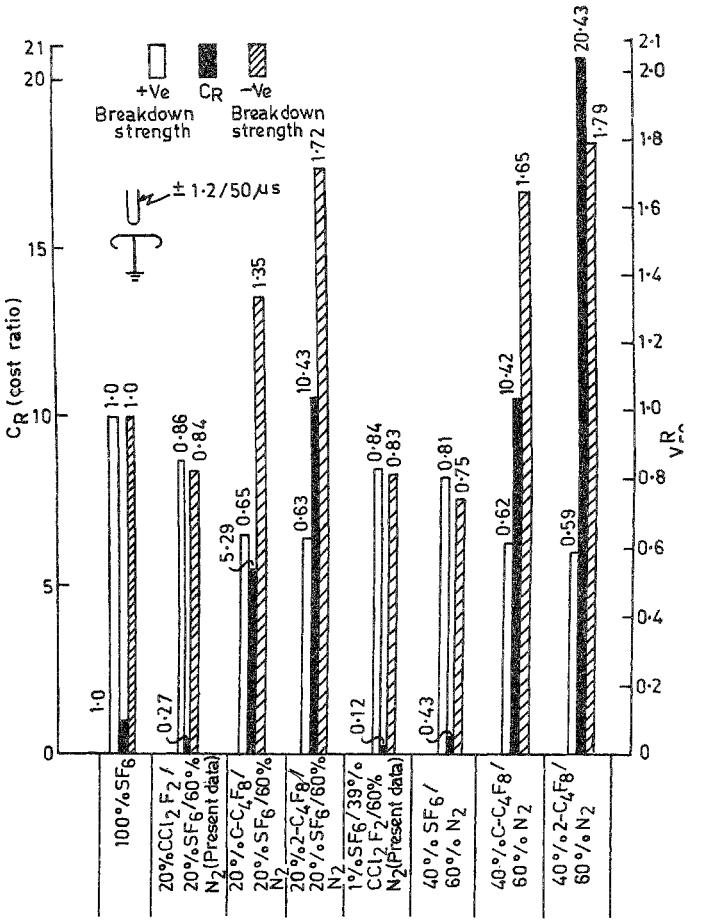

FIG 1. Histograms of the relation between cost ratio (C_R) and impulse breakdown strength ratio (V^R_{50}) for positive and negative rod–plane gaps for different binary and ternary gas mixtures, at a pressure of 0·3 MPa at a gap of 20 mm.

giving a dielectric strength of about 0·83 to 0·86 relative to pure SF_6 (1·0). However, it is also seen from the figure that the use of perfluorocarbon compounds in place of CCl_2F_2 in ternary mixture will give the highest cost ratio between 5·0 and 20·0 compared to SF_6 (cost of ratio = cost of the mixture/cost of SF_6). The analysis clearly shows that a 30% SF_6/10% CCl_2F_2/60% CO_2 mixture costs only 33% of the cost of the pure SF_6 but gives typically 110 to 170% positive breakdown strength, and 90 to 110% negative breakdown strength as compared to that of pure SF_6 depending on the mixture pressure over the range of pressures investigated (1 to 5 bar). Also, these $SF_6/CCl_2F_2/CO_2$ mixtures are very effective in suppressing carbon formation after the breakdown. Some important correlations between critical electric fields, EC and non-uniform field behaviour of the gases and gas mixtures (binary and ternary) studied under impulse voltage stresses have been deduced. These relations are useful for a proper interpretation of the breakdown strength of gas mixtures and for identifying the most suitable gas mixture for a given application.

Most of the data presented in the work have been obtained for the first time and appear to be of great practical significance.

References

1. MALLER, V. N. AND NAIDU, M. S. — *Advances in high voltage insulation and arc interruption in SF_6 and vacuum*, 1981, Pergamon Press.
2. DALY, S. J. AND HOPKINS, M. D. — Methods of particle control in SF_6 insulated CGIT systems, *IEEE Trans.*, 1982, **PAS-101**, 1654-1662.
3. BAKKEN, J. A. — Determination of characteristic voltages in impulse and switching surge testing, *IEEE Trans.*, 1967, **PAS-86**, 962–968.
4. PAI, R. Y. AND CHRISTOPHOROU, L. G. — *VIIth Int. Conf. on Gas Discharges*, London, 1980, pp 232–235.

Thesis Abstract (Ph.D.)

Laser Raman studies of an adiabatic expansion by T. G. Nagaraju.
Research supervisor: C. R. Prasad.
Department: Mechanical Engineering.

1. Introduction

Identification and measurement of concentrations of constituent species and temperature fields are essential for monitoring the performance of practical devices and also for formulation and assessment of analytical models in many situations such as in high-speed gas flows, combustion, aerodynamics, etc. Conventional diagnostic techniques like microprobe analysis for concentrations or thermometric probes for temperature cause aerodynamic and thermal distortions and also influence the sample by quenching, catalysis and radical recombination. Optical methods like spectroscopy and pyrometry, although non-perturbing, suffer from poor spatial resolution and give only averages along optical path. On the other hand, optical techniques based on Rayleigh or Raman[1] (spontaneous and coherent) scattering and fluorescence do not have these drawbacks and hence scattering has become a very powerful diagnostic tool with the availability of high-powered lasers, and has been demonstrated to be very effective in investigations of fluid flows[2], combustion analysis, both in the lab and in engines[3,4], meteorology, atmospheric pollution monitoring[6], humidity and temperature measurement[7] and even surface temperature of oceans and so on.

In this work, the development of a laser Raman scattering system for laboratory measurement of species concentrations and temperatures in an expansion chamber is described.

2. Experimental set-up and procedure

Schematic of the experimental set up is shown in Fig. 1. The dye laser is flash lamp pumped emitting pulses of 10–50μs with powers up to 10 kW at 595 nm, with rhodamine 590 as the dye. A 0·5-m Czerny-

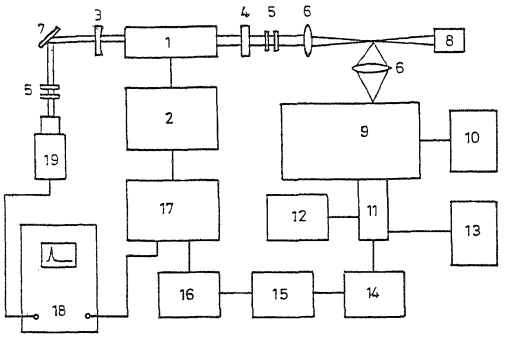

FIG 1. Schematic layout for detection of laser Raman scattered light by photon counting

Turner monochromator with in-line optics was built for dispersing the Raman scattered light. A stepper motor actuates the sine bar drive of the grating and also provides a direct wavelength readout The signal intensity is extremely low since the spontaneous Raman scattering cross-section is very small. Hence, an efficient optical system for collecting scattered light has been employed and a photon counter comprising a cooled photomultiplier (RCA C31034) followed by a fast pulse amplifier, discriminator and counter was utilized for measuring its intensity An expansion chamber consisting of two cylindrical vessels with a latex rubber diaphragm in between was built for carrying out rapid adiabatic expansions The bottom vessel equipped with quartz windows for optical probing holds the gas to be expanded, while the other vessel is suddenly communicated with a vacuum reservoir to perform rapid expansions

The intensity of light scattered at the Raman-shifted wavelength w_{η} by a species j having number density N_j is

$$I(w_r) = I(w_0)\ N_j \Omega K\ (d\sigma/d\Omega)_j$$

where $I(w_0)$ is intensity of exciting laser and Ω the solid angle of collection Species concentrations N_j are obtained by taking ratios of the photon counts n_j (given by $n_j = A\ (w_{\eta}) \cdot I(w_{\eta})$, where $A(w_{\eta})$ is a system constant), with that for nitrogen n_n whose concentration is known and remains unchanged. Temperature

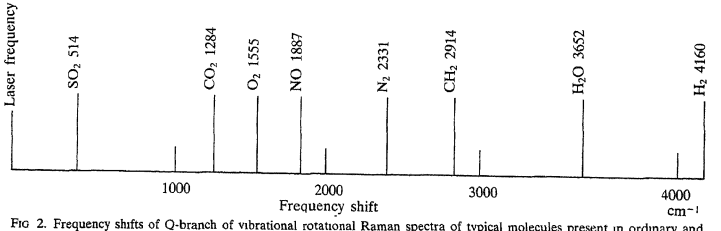

FIG 2. Frequency shifts of Q-branch of vibrational rotational Raman spectra of typical molecules present in ordinary and polluted atmosphere relative to the exciting laser frequency.

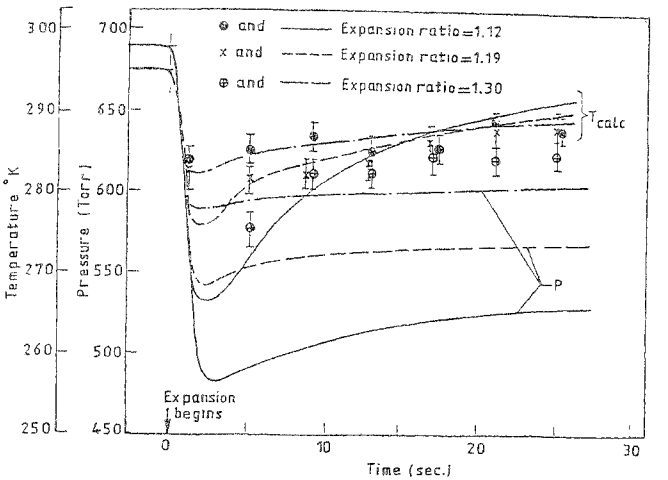

Fig 3 Expansion of dry air. Values of P shown are the pressure measured with pressure transducer T_{calc} is the average temperature calculated from P values. Points are the Raman temperature derived from ratios of the measured Raman scattered intensities

is found by taking intensity ratios of two rotational lines in the pure rotational Raman spectrum of nitrogen. A computer program for computing the Raman spectrum has been developed and with its help the optimum wavelengths, λ_1 and λ_2 are chosen so that the temperature is inferred from the ratio of two intensities.

$$R = I(\lambda_1)/I(\lambda_2)$$

(where $I(\lambda_1)$ and $I(\lambda_2)$ are the photon counts at locations λ_1 and λ_2) so that the error is minimum It has been shown that the relationship between the ratio of intensities and temperature is

$$\ln R = A + \frac{B}{T}, \text{ where } A \text{ and } B \text{ are constants.}$$

By measuring the ratio of intensities, the temperature can be determined.

3. Results

Figures 3 and 4 show the experimental results of adiabatic expansion of dry air and air saturated with water, respectively. The temperature measured by the rotational Raman scattering has an error bar of ± 2°C; the expected error from the analysis in locating λ_1 and λ_2 is about 0·16% in $\Delta T/T$, *i.e*, about ± 0·5°C. Thus the total error in the T_{Raman} measured is about ± 2·5°C which is acceptable

In the same figures, T calculated and temperature indicated by the thermocouple are shown for comparison

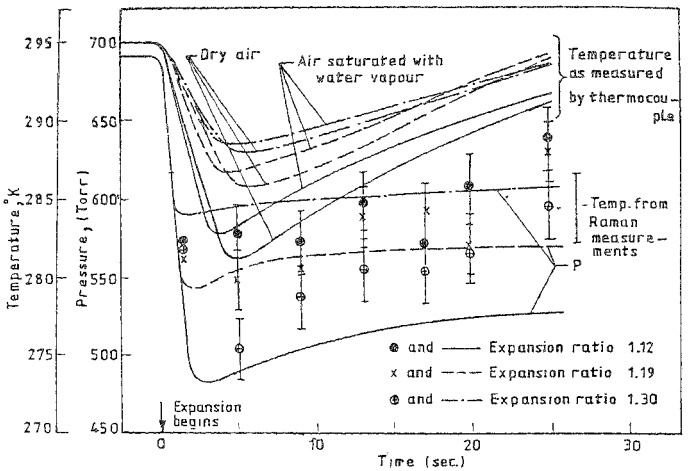

FIG 4 Expansion of air saturated with water vapour Measured values of P shown here do not differ significantly from those in Fig. 3 Temperature measured by the thermocouple located at the centre of the vessel is plotted.

References

1 HARTLEY, D L , HARDESTY, D R., LAPP, M , DOOHER, J AND DRYER, F D (eds) — In *Efficient use of energy*, AIP Conf Proc #25, American Institute of Physics, 1975, p 153

2 KILLINGER, D. K AND MOORADIAN, A (eds) — *Optical and laser remote sensing*, Springer Series in Optical Sciences, Vol 39, 1983, Springer-Verlag

3 ECKBRETH, A C , BONCZYK, P A AND VERDIECK, J. F — Combustion diagnostics by laser Raman and fluorescence techniques, *Prog Energy Combust Sci* , 1979, 5, 253–322

4 LAPP, M , PENNEY, C M. AND ASHER, J. A — *Application of light scattering techniques for measurements of density, temperature and velocity in gas dynamics*, ARL Report, #ARL-73-0045, 1973

5. MELFI, S H AND WHITEMAN, D — Observation of lower atmospheric moisture structure and its evaluation using a Raman lidar, *Bull Am Met Soc* , 1985, **66**, 1288–1292

6. INABA, H — Detection of atoms and molecules by Raman scattering and resonance fluorescence, *Laser monitoring of the atmosphere* (E D Hinkley, ed.), Topics in Applied Physics, Vol 14, 1976, Springer-Verlag.

7. POURNY, J C , RENAUT, D AND ORSZAG, A — Raman-lidar humidity sounding of the atmospheric boundary layer, *Appl Opt.*, 1979, **18**, 1141–1148

8 LEONARD, D. A., CAPUTO, D. AND HOGE, F. E — Remote sensing of subsurface water temperature by Raman scattering, *Appl Opt* , 1979, **18**, 1732–1745

Thesis Abstract (Ph.D)

Basic studies on electrochemical power sources: voltage transients, alternating curren impedance and steady-state discharge characteristics of magnesium-manganese dioxid dry cells (with supplementary investigations on titanium-substrate cobalt oxide anc magnetite anode development for electrosynthesis) by S. R. Narayanan.
Research supervisor: S. Sathyanarayana.
Department: Inorganic and Physical Chemistry.

1. Introduction

Primary batteries based on reactive metal anodes such as magnesium and lithium are becoming increasingly important. Such batteries have relatively a high energy density and a long shelf-life compared to conventional zinc–manganese dioxide (Leclanché) dry cells. The long shelf-life is mainly due to the presence of a protective passive film, on the surface of the anode, produced during the fabrication of the cells or by the reaction of the anode with the cell electrolyte. While inadequate passivation of the anode leads to premature failure of the cells by corrosion of the anode, an excessive passivation of the anode results in a long delay time for the attainment of steady-state cell voltage after the initiation of discharge, due to the difficulty of anode film breakdown. An optimal passivation treatment is therefore that which produces a protective film with a minimal voltage delay during discharge

The shelf-life and voltage-delay of magnesium–manganese dioxide dry cells are mainly governed by physical and electrical properties of the film-covered anode/solution interface[1,2]. It is therefore of great practical importance to evolve techniques which will determine the properties of the film-covered anode.

A galvanostatic pulse method has been proposed by Moshtev *et al*, to determine film resistance and capacitance of lithium anodes in Li-SO_2 and Li-$SOCl_2$ primary cells[3,4] This work, however, has several limitations. The film capacitance is calculated from the initial slope of a galvanostatic high current, short discharge pulse, and film resistance is obtained from the steady-state over-voltage observed during a galvanostatic smaller current, longer discharge pulse Such a sharp division of the cell response to pulse excitation is arbitrary since it amounts to a purely non-faradaic current flow at the anode during the short pulse (few μs), and depending on both the nature of the anode metal and the state of passivation, the parameters and time constants governing the faradaic and non-faradaic processes will be different. Further, pulse excitation involves a fairly high current density (1-100 mA cm^{-2} for D-size cells) which may lead to dielectric breakdown of the film, especially in the short-pulse experiments.

Povarov *et al*[5] have studied the lithium/solution interface by impedance method. However, no special precautions have been taken in their experiments to eliminate the possibility of the breakdown of anode film. Further, the interpretation of data does not consider all plausible equivalent circuit representations for the lithium anode/solution interface.

In the light of these observations, we felt it desirable to carry out measurements at currents sufficiently small to eliminate any dielectric damage to the passive film on the anode, compare the experimental results with the theoretical behaviour of several plausible electrical equivalent circuits and thereby identify the description that fits the physical situation best. This would also lead to the evaluation of electrochemical parameters which govern the physicochemical processes at the anode/solution interface. Such studies were not found in literature.

2. Present investigation

In the present investigation, a technique has been developed to evaluate the fundamental electrochemical properties of the anode solution interface in magnesium–manganese dioxide (Mg–MnO_2) dry cells. The method is based on the measurement and interpretation of:

(i) voltage transients observed when the cells are discharged galvanostatically at current densities so small as to cause no anode film breakdown[6].

(ii) impedance parameters obtained under low-amplitude sinusoidal excitation, the perturbation of cell voltage being kept so low as to make the measurements non-destructive as in case (i) above

(iii) steady-state discharge characteristics under galvanostatic conditions after film breakdown.

Based on the physiochemical processes which prevail during the above experiments, four plausible electrical equivalent circuit models for the anode/solution interface have been proposed, theoretically analysed and criteria evolved to compare the experimental data with theory. It has been shown that the treatment of the data by the theoretical approach developed permits the determination of the most plausible equivalent circuit representation for the physical situation under study, and allows complete evaluation of the electrochemical parameters for the film-covered anode.

In the course of investigations on the discharge characteristics of Mg–MnO_2 dry cells at the usual rates of discharge, it was found that the voltage delay, when the cell is discharged at ambient temperature and at a constant current, is three to four times less than that when discharged across an equivalent constant resistance. While the constant current mode of discharge is the one usually employed for laboratory tests, the constant resistance mode is the more commonly used mode in cell applications Therefore, a theoretical and experimental investigation has been carried out to inter-relate voltage transients exhibited during the two modes of discharge.

3. Supplementary investigations on titanium-substrate cobalt oxide and magnetite anode development for electrosynthesis

In the choice of anodes for electrochemical processes the phenomenon of anodic dissolution rules out all but a very few materials The 'insoluble anodes' which are in vogue are largely based on titanium metal coated with Pt, RuO_2, PbO_2 and so on. There is a continuous effort to replace the precious metals by base-metal oxide coatings. Cobalt oxide-coated titanium anodes are electrocatalysis for the oxidation of chloride to chlorate, and the reported methods of preparation involve the pyrolysis of cobalt nitrate at 300°–400°C[7]. It is known that if the temperature of preparation is lowered the number of defect states is larger and thus the electrocatalytic activity is higher[8]. Therefore, it was considered desirable to investigate preparation techniques which employ lower temperatures. In the course of the present investigation an electrochemical technique has been developed to produce an adherent and conducting coat of cobalt oxide on titanium. The method involves anodic oxidation of cobalt ions on titanium from cobalt nitrate at ~ 90°C. The conditions for obtaining deposits with good adhesion and desirable morphology have been identified. Preliminary investigation of the electrochemical polarisation characteristics prove it attractive for the oxidation of chloride to chlorate. It has also been found effective in the electrochemical destruction of cyanides. Preliminary studies using x-ray powder diffraction and thermal decomposition methods indicate the deposits to be composed largely of CoOOH

It is known that failure of anodes based on titanium substrate is usually due to the build-up of a barrier-type TiO_2 film at the substrate/coating interface. This is generally mitigated during preparation by rendering the insulating oxide conducting with dopants such as Pt, RuO_2, etc. Here again, to substitute the precious metal by base-metal oxides, the applicability of conducting SnO_2–SbO_x coatings has been investigated. Preliminary studies with these interfacial coatings have shown satisfactory results Thus the SnO_2–SbO_x under-coat combined with an exterior coat of base metal oxides such as cobalt oxide is projected as a viable alternative to anodes based on precious metal and precious metal oxides

Since magnetite, Fe_3O_4, is inexpensive, non-toxic and has proven electro-chemical properties, the feasibility of coating magnetite on titanium has been investigated. Methods of coating which have been studied in this work are the following:

1. Direct methods of coating based on
   (a) electrochemical cathodic deposition of Fe_3O_4 from aqueous solutions containing Fe^{3+},
   (b) electrophoretic application of colloidal Fe_3O_4.
2. Indirect methods involving plating of iron on titanium and subsequent oxidation of Fe_3O_4 by the following methods:
   (a) anodic polarisation in alkaline bath containing chlorides;

(b) oxidation in alkaline nitrate melt,

(c) steam oxidation,

(d) hydrothermal oxidation.

Although all the above methods yielded a coating of Fe_3O_4, none of them was satisfactory, generally due to the poor adhesion to the substrate. Excessive oxidation of the substrate was encountered when the coatings were adherent

Considering the variety of methods investigated, the coating Fe_3O_4 still poses a challenge. A method using plasma spraying has however been reported in literature[9], but it is not clear as to whether it mitigates the problems faced in the methods examined in the present study

References

1 RATNAKUMAR, B V. AND SATHYANARAYANA, S — *J Power Sources*, 1983, **10**, 219–241

2 SATHYANARAYANA, S AND RATNAKUMAR, B V. — *J. Power Sources*, 1983, **10**, 243–261

3 MOSHTEV, R. V , GERONOV, Y AND PURUSHEVA, B. — *J. Electrochem. Soc* , 1981, **128**, 1851–1857

4. MOSHTEV, R. V AND GERONOV, Y. — *J Power Sources*, 1982, **8**, 395–401

5 POVAROV, YU M *et al* — *Electrokhimiya*, 1980, **16**, 1768–1772. 1983, **19**, 586–593, 1982, **18**, 1160–1169

6 NARAYANAN, S R. AND SATHYANARAYANA, S — *J Power Sources*, 1985, **15**, 27–43.

7 LYUBUSHKIN, V I AND LYUBUSHKINA, E T. — *Zh Prikl. Khim.*, 1980, **53**, 2224–2228

8 SHALAGINOV, V V. *et al* — *Electrokhimiya*, 1983, **19**, 537.

9. FUJII, T , KODAMA, T , BABA, H AND KITAHARA, S — *Trans. Natn Res Inst Metals*, 1983, **25**, 16–21.

Thesis Abstract (Ph.D.)

Norrish type I α-cleavage reaction of cyclobutanethiones and selectivity in photochemical reactions using cyclodextrin by B. Nageshwar Rao.
Research supervisors: V. Ramamurthy and S. N. Balasubramanyam.
Department: Organic Chemistry.

1. Introduction

The results obtained during photochemical studies on cyclobutanethiones and cyclodextrin complexes of various substrates have been divided into two parts. Part I deals with the photochemical α-cleavage reactions of strained 1,3-bichromophoric cyclobutanethiones and theoretical investigations (MINDO/3 method) on the mechanism of the α-cleavage reaction of cyclobutanethiones. Part II deals with the modification of photoreactivity of dibenzyl ketones, benzyl phenyl esters, α-alkyl dibenzyl ketones and phenyl esters in cyclodextrin *via* inclusion complex formation.

2. Discussion

The photochemical α-cleavage reaction of 1,3-bichromophoric cyclobutanethiones **1–7** (Scheme 1) has been established. The reactive state is deduced to be n, π^{*3}. The formation of rearrangement products and solvent adducts suggests the intermediacy of 1,4-diradicals (**8–9**) and thiacarbenes (**10–11**) in this reaction[1,2].

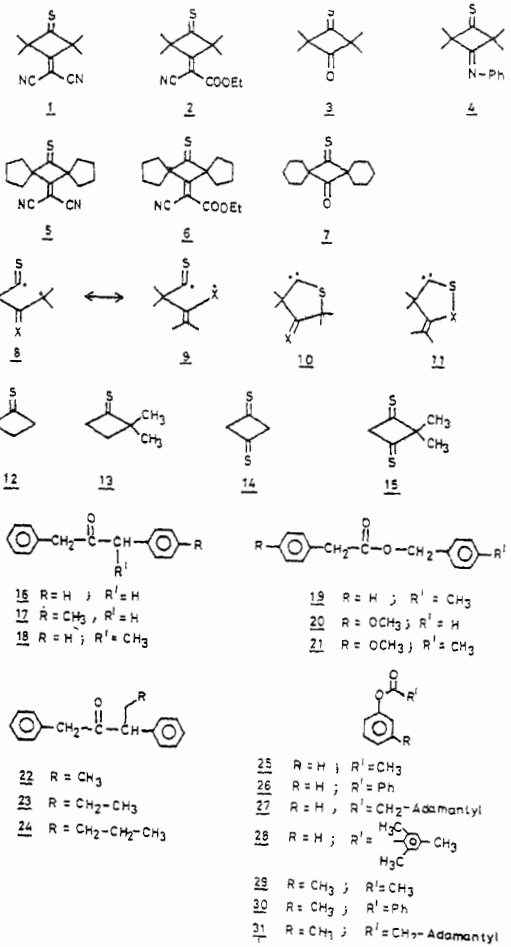
1
2
3
4
5
6
7
8
9
10
11
12
13
14
15
16 R = H ; R' = H
17 R = CH3 , R' = H
18 R = H ; R' = CH3
19 R = H ; R' = CH3
20 R = OCH3 ; R' = H
21 R = OCH3 ; R' = CH3
22 R = CH3
23 R = CH2-CH3
24 R = CH2-CH2-CH3
25 R = H ; R' = CH3
26 R = H ; R' = Ph
27 R = H , R' = CH2-Adamantyl
28 R = H ; R' =
29 R = CH3 ; R' = CH3
30 R = CH3 ; R' = Ph
31 R = CH3 ; R' = CH2-Adamantyl

Scheme 1.

Two pathways for the formation of thiacarbene intermediate are considered (1) the two canonical forms of the first-formed triplet diradical undergo ring expansion to give thiacarbene, (n) concerted formation of thiacarbene from the n, π^{-1} excited state of thiones, at least in part, for the formation of one of the thioacetals Characterization of products and the mechanism of their formation are discussed

A theoretical study of the mechanism of α-cleavage reaction of cyclobutanethiones (**12–15**) has been conducted using the UHF MINDO/3 formalism[3] Thermodynamic feasibility of interconversion of n, π^{*3} and two potential primary products, *viz* , the 1,4-diradical and the cyclic thiacarbene was examined based on the computed energies for these structures. Electronic feasibility of the reaction pathways was also considered with the help of Salem's state correlation approach in conjuction with MINDO/3 energies Finally, the kinetic feasibility was investigated by approximately locating the transition states for different modes of reaction

The n, π^* triplet of unsubstituted cyclobutanethione is indicated not to undergo α-cleavage to the 1,4-diradical on energetic grounds However, the process should be possible in **13** since the introduction of gem-dimethyl group at C_2 stabilizes both the diradical and the transition state leading to it For both **12** and **13**, direct rearrangement of triplet thione to the thiacarbene is thermodynamically favourable, but involves a prohibitively large barrier

The α-cleavage process for triplet cyclobutanedithione **14** is facilitated by a greater ring strain relief as well as by thiaallylic stabilization on going to the diradical. Gem-dimethyl substitution favours the process further. Rearrangement of the triplet to the thiacarbene is calculated to be feasible for the dimethyl dithione **15**, but not for unsubstituted dithione **14** The calculated results are consistent with experimental observations on related thiones. The study provides an understanding of the role of alkyl substituents in modifying the intrinsic reactivity preferences of small ring thiones

The photochemical behaviour of dibenzyl ketones (**16–18**) and benzyl phenyl esters (**19–21**) in hosts deoxycholic acid (DCA), Dianin's compound and cyclodextrin (CD)[4] in the solid state has been investigated. These guest molecules undergo α-cleavage reaction and give coupling products AA, AB and BB[5] Excitation of the above guest molecules in the solid inclusion complexes produces cage product AB in quantitative yields These results suggest that the translational motion of the benzyl radical pairs is restricted in all the three media. Rearrangement products were formed upon photolysis of **16–18** in Dianin's compound and CD and were absent in *DCA* The absence of rearrangement product in *DCA* and its presence to varied extents in Dianin's compound and CD is suggested to be an indication of the restriction imposed by the host on the reorientational process of geminate radical pairs

The photoreactivity of α-alkyl dibenzyl ketones (**22–24**) in CD has been investigated The existence of various conformations of these guest molecules in organic solvents leads to the occurrence of both type I and type II reactions In solid CD complexes, the excited guest molecule selects only the type I reaction pathway. The total absence of type II reaction in solid CD complexes is attributed to the binding of an unfavourable conformation for the type II reaction in CD cavity In aqueous CD solution, the cage product AB is accompanied by another product, resulting from the rearrangement of geminate radical pair The inclusion complex formation between guests (**22–24**) and aqueous CD was identified by spectroscopic techniques (^{1}H–nmr and fluorescence emission spectroscopy) Fluorescence emission spectra were used to calculate the dissociation constants of these complexes in aqueous medium. Based on the differences in chemical shifts of CD protons after complexation and product distribution in CD complexes, the probable conformation of the molecule inside the cyclodextrin cavity is discussed

The effect of CD encapsulation on the photo-Fries rearrangement of phenyl esters[6,7] (**25–31**) has been studied. Photochemical studies of phenyl esters in homogeneous solution are briefly reviewed. In organic solvents, direct excitation of phenyl esters (**25–28**) results in the formation of *ortho* and *para*-acylated phenols and *m*-methylphenyl esters (**29–31**) produce two *ortho*- and one *para*-acylated phenols. High *ortho* selectivity is observed for phenyl esters **25–31** in both aqueous and solid CD complexes *m*-Methylphenyl esters further showed regioselectivity by giving 2-acyl, 5-methyl phenols as major products Regioselectivity is found to be dependent upon the size of the acyl group in aqueous CD solution. Observed *ortho*

selectivity and regioselectivity are explained based on the geometry of the complex. Existence of complexes in aqueous solutions is inferred from ^{1}H-nmr and in the solid state from x-ray powder photographs.

References

1 MUTHURAMU, K AND RAMAMURTHY, V — *J Org Chem*, 1980, **45**, 4532–4533

2 MUTHURAMU, K AND RAMAMURTHY, V — *J Chem Soc. Chem Commun*, 1980, 243–244

3 BINGHAM, R C, DEWAR, M J S AND LO, H D — *J Am Chem Soc*, 1975, **97**, 1285–1311

4 BENDER, M L AND KOMIYAMA, M — *Cyclodextrin chemistry*, 1978, Springer

5 QUINKERT, G, OPTIZ, K, WIERSDORFF, W AND WEINLICH, J — *Tetrahedron Lett*, 1963, 1863–1868

6 ANDERSON, J. C AND REESE, C B — *Proc Chem Soc*, 1960, 217

7 KOBSA, H — *J Org Chem*, 1962, **27**, 2293–2298

Thesis Abstract (Ph.D.)

Novel layered and network metal oxides: synthesis and characterization by Vasudeva Bhat.
Research supervisor: J. Gopalakrishnan.
Department: Solid State and Structural Chemistry Unit.

1. Introduction

Transition metal oxides play a vital role in various fields of science and materials technology owing to a variety of properties exhibited by them. Among these, oxides with lamellar structures, such as clay minerals, were known for a long time showing interlayer properties which are being exploited in their use as ion-exchangers and catalysts. Besides their technical applications, layered materials are also important from basic scientific point of view, because they provide low-dimensional model solids to investigate intercalation and magnetic and electrical properties in low dimensions. A part of the present research work has been devoted to preparation of layered oxides and investigation of their intercalation behaviour.

It is not always possible to synthesize new materials by conventional methods owing to the inherent limitations arising from thermodynamics and kinetics at high temperatures. One then looks for alternative preparative strategies. Low-temperature preparative methods have become popular in recent years which enable synthesis of many new solids. We have employed some low-temperature methods to prepare several new oxides.

2. Experimental and discussion

New series of layered perovskite oxides of the general formulae i) $ALaNb_2O_7$ and ii) $ALa_2NbTi_2O_{10}$ (A = Li, Na, K, Rb, Cs, NH_4), constituting, respectively, $n = 2$ and $n = 3$ members of the family $A[A'_{n-1}B_nO_{3n+1}]$ have been identified. Oxides with A = K, Rb and Cs were synthesized by the ceramic method. Other members with A = H, Li, Na and NH_4 were prepared by topotactic ion exchange starting from the K-analogue. Their structure consists of n perovskite slabs interleaved by the A ions. The stacking of the perovskite slabs in the c-direction depends on the nature of A cation. The stacking sequences are analogous to those found in the corresponding $ACa_2Nb_3O_{10}$ compounds[1].

Several members of a new series of Ruddlesden–Popper phases of the general formula $A_2Ln_2Ti_3O_{10}$ (A = K or Rb, Ln = La, Nd, Sm, Gd or Dy) which are related to $Sr_4Ti_3O_{10}$[2,3] were synthesized employing

ceramic method. Corresponding hydrates were formed on exposing these oxides to humid atmosphere. Exchange of K^+ in $K_2La_2Ti_3O_{10}$ by Li^+ or Na^+ in molten nitrates yields anhydrous Li and Na analogues. Proton exchange of K^+ in $K_2La_2Ti_3O_{10}$ yields layered $H_2La_2Ti_3O_{10}$. Anhydrous $A_2Ln_2Ti_3O_{10}$ consists of 3-octahedra-thick, (001)-cut perovskite slabs, $Ln_2Ti_3O_{10}$, stacked along c-direction with alternate slabs being shifted by $(a+b)/2$; in monohydrates ($A_2Ln_2Ti_3O_{10}.H_2O$), adjacent slabs are not shifted in ab-plane. The defect perovskite, $La_{2/3}TiO_3$, is obtained by the decomposition of $H_2La_2Ti_3O_{10}$.

Another new type of rutile-related layered oxide has been identified. Layered $HMWO_6.1{\cdot}5H_2O$ (M = Nb or Ta) were synthesized from $LiMWO_6$ by topotactic proton exchange of lithium. A structural model is proposed for the parent $LiMWO_6$ and the protonated derivatives. The structure consists of MWO_6 sheets made up of M/W-oxygen octahedra with rutile-like edge and corner sharing. In $LiMWO_6$, such sheets are stacked exactly one above the other in the c-direction, whereas in $HMWO_6.1{\cdot}5H_2O$, alternate MWO_6 sheets are displaced laterally. Layered $ANbWO_6.H_2O$ (A = Li, Na, K, and Tl) are also prepared by ion exchange starting from $HNbWO_6.1{\cdot}5H_2O$. Anhydrous $ANbWO_6$ (A = Li, Na, K or Tl) obtained by dehydration of the hydrates reveals that three different structures, *viz*, rutile-like, TTB-like and pyrochlore, are competitive for the $ANbWO_6$ composition depending on the radius of the A cation.

Intercalation behaviour of the layered protonated oxides, $HNbWO_6$, $HLaNb_2O_7$ and $HLa_2NbTi_2O_{10}$ were studied. $HNbWO_6$, for example, intercalates several *n*-alkylmonoamines, *n*-alkyl diamines, pyridine and aniline. Monoamines seem to form bilayers, whereas diamines form monolayers in the interlayer region. Pyridine molecules form monolayers with the ring planes oriented parallel to the surface of $NbWO_6$ sheets, whereas aniline molecules form bilayers.

Oxidative extraction and proton exchange of lithium in β-Li_2MoO_3 yield metastable oxides. A new solid solution series, $Li_{2-x}MoO_3$ ($0 < x < 1{\cdot}5$), possessing a β-Li_2MoO_3-like 'layered' structure has been identified. Complete delithiation of Li_2MoO_3 results in the formation of a poorly crystalline MoO_3. Topotactic exchange of Li^+ in Li_2MoO_3 by protons using dilute H_2SO_4 yields H_2MoO_3.

Reductive insertion of electropositive metals, such as Na, K, Ba into oxide hosts such as WO_3, MoO_3 or V_2O_5 provides a new method for the synthesis of oxide bronzes. The insertions are carried out by the reaction of the host oxide with the iodides of the electropositive metals. This method enables the synthesis of not only the known bronzes but also new ones that cannot be made by conventional methods.

ReO_3-like $LiMWO_6$ (M = Nb or Ta) were formed on treating $LiMWO_6$ with hot aqueous H_2SO_4. The reaction is accompanied by a structural transformation from the rutile to the ReO_3 structure which seems to occur through a dissolution–recrystallization mechanism. $HMWO_6$ phases yield $H_{1+x}MWO_6$ hydrogen bronzes on exposure to hydrogen in the presence of platinum catalyst. We have also carried out topotactic hydrogen insertion in perovskite oxides, $LaNiO_3$ and $LaCoO_3$.

References

1 Dion, M., Ganne, M. and Tournoux, M. — *Mater. Res. Bull.*, 1981, **16**, 1429–1435.

2 Ruddlesden, S. N. and Popper, P. — *Acta Cryst.*, 1957, **10**, 538–539.

3 Ruddlesden, S. N. and Popper, P. — *Acta Cryst.*, 1958, **11**, 54–55.

Thesis Abstract (Ph.D.)

Investigations of high-T_c oxide superconductors and related oxide systems by electron microscopy and cognate techniques by L. Ganapathi.
Research supervisor: C. N. R. Rao.
Department: Solid State Structural Chemistry Unit.

1. Introduction

Characterization forms an essential aspect of all investigations dealing with solids. The important aspects

of characterization are chemical composition and compositional homogeneity, structure and lastly identification and analysis of defects and impurities influencing the properties of the material[1] Nonstoichiometry and extended defects are becoming well known in solid-state chemistry The conventional idea of point defects no more explains the diverse class of compounds exhibiting apparent nonstoichiometry The formation of crystallographic shear planes and disordered intergrowth are known to be two major types of extended defects arising in the case of nonstoichiometry in transition metal oxides[2] Ordered intergrowth between different structures offers immense scope for manipulating new class of compounds with desired properties

Although of recent origin, high-temperature superconductivity has gained independent status as a branch of science[3] The structural chemistry associated with these high-T_c oxides is rather traditional in solid-state chemistry, especially their stoichiometry playing a pivotal role in determining their properties Three major classes of these high-T_c superconductors are investigated in the light of their structure and stoichiometry.

This work comprises preparation and characterization of the new high-T_c materials and some other novel metal oxides. X-ray diffraction, electron microscopy and thermogravimetry have been extensively used in the characterization of these oxide materials. In particular, electron microscopy has been employed to examine not only the crystal structure but also the local structure of many of the oxide materials

2. Experimental

High-T_c oxide superconductors were prepared by the ceramic route involving high-temperature reactions of the component oxides and/or carbonates. Repeated grinding and heating were followed till the desired products were obtained Compounds with various oxygen stoichiometries were obtained by heating in varied oxygen partial pressures. β-aluminas and related oxides were prepared by conventional solid-state reaction The $La_{n+1}Ni_nO_{3n+1}$ members were prepared by a precursor route[4]. The $n = 4$ and 5 members of the $(NaCa)_nNb_nO_{3n+2}$ system were prepared starting from the respective metal oxides or carbonates The intermediate members ($4 < n < 4{\cdot}5$) were prepared by the reaction of appropriate mixture of the $n = 4$ and $n = 5$ members. The solid-solution hydrates, $W_{1-x}Mo_xO_3{\cdot}H_2O$, were precipitated by adding an ammoniacal solution of appropriate amounts of WO_3 and MoO_3 into concentrated nitric acid On dehydration they gave homogeneous solid-solution oxides $W_{1-x}Mo_xO_3$ The reduced solid-solution oxides of the type W_{1-x}, $Mo_xO_{3-\delta}$ were prepared by reducing the solid-solution oxides in a dilute hydrogen atmosphere (1:20 mixture of H_2 and N_2). $K_yW_{1-x}Mo_xO_3$ bronzes were prepared by the reaction of potassium iodide with solid-solution oxides in dynamic pumping conditions[5].

X-ray diffraction patterns were recorded with a Jeol JDX–8P diffractometer. Thermogravimetry was carried out using a Sartorious microbalance Electrical resistivity measurements were carried out by four-probe dc method Electron microscopy was carried out using a Jeol JEM–200 CX electron microscope in top-entry configuration The details of sample preparation and operating conditions are given elsewhere[6]

3. Results and discussion

A number of compositions in $YBa_2Cu_3O_{7-\delta}$ system were studied by thermogravimetry to understand the nature of oxygen discharge and intercalation The variation of stoichiometry in $YBa_2Cu_3O_{7-\delta}$ with structure has been investigated in detail It is shown that the orthorhombic structure of $YBa_2Cu_3O_{7-\delta}$ changes over to the tetragonal structure around $\delta = 0{\cdot}6$. The superconducting transition temperature, T_c, is shown to be 90 ± 5K when $\delta \simeq 0{\cdot}1$ Variation of T_c with δ shows a plateau ($T_c = 50 \pm 10$K) when $0{\cdot}2 < \delta = 0{\cdot}4$. It is suggested that this behaviour of superconductivity with δ may be due to a changeover from chain-superconductivity to sheet-superconductivity Electron microscopy has been employed to investigate $YBa_2Cu_3O_{7-\delta}$ with special emphasis on the twins observed in them High-resolution image of twins suggests an oxygen-rich interface across which the $[CuO_2]$ planes change their orientation accompanied by an interchange of a and b axes

$La_{3-x}Ba_{3+x}Cu_6O_{14+\delta}$ compositions are found to generally possess a tetragonal structure with excess oxygen; the tetragonal cell is based on a cubic perovskite subcell and triple periodicity. $LaBa_2Cu_3O_{7-\delta}$ compositions have a tetragonal structure when δ deviates from zero and the tetragonal structure is similar to

that of $La_{3-x}Ba_{14+x}Cu_6O_{14+\delta}$. Electron micrographs of these tetragonal oxides show 90° microdomains. Orthorhombic $LaBa_2Cu_3O_{7-\delta}$ with high T_c (77K) is found only when $\delta = 0{\cdot}0$ and this sample shows twins

Oxides of the general formula $(Bi_2O_2)^{2+}$ $(A_nB_nO_{3n+1})^{2-}$, where A = Bi or Ba, B = Ti, Fe, W and n = number of perovskite layers, have been investigated by high-resolution electron microscopy. Lattice images obtained for the n=1 to 6 members show stacking of $n - 1$ perovskite layers sandwiched between dark bands due to the $(Bi_2O_2)^{2+}$ layers. It has been possible to resolve the perovskite layer structures in some of the oxides. A highly ordered structure is observed up to $n = 3$ member, whereas higher members show superstructures, dislocations and stacking faults arising from the side-stepping of $(Bi_2O_2)^{2+}$ layers

Structure, stoichiometry and superconductivity of oxides of the Bi-Ca-Sr-Cu-O system have been investigated employing a variety of techniques. These rare-earth-free cuprates show onset of superconductivity around 100K. Their structure bears similarities with those of the Aurivillius family of oxides. Two phases with c 24 A and c 31 A have been identified based on diffraction studies. Electron microscopy shows an incommensurate superlattice along the b-axis in all these oxides. $Bi_4Ca_2Sr_3Cu_4O_x$ shows a distinctive resistivity anomaly around 200K suggesting the presence of a small fraction of a very high-T_c material. This composition showed the presence of different c parameters in a few crystals suggesting a possible correlation between high-T_c and intergrowth structures

High-resolution electron microscopic (HREM) investigations of potassium β-alumina and related gallate and ferrite have been carried out. Whereas the aluminate and gallate are highly disordered consisting of random sequences of β and β″ units, the ferrite is more ordered. The aluminate and gallate are susceptible to electron beam damage just as sodium β-alumina. The ferrite is however beam-stable. Difference in behaviour of these related oxides probably arises from the different mechanisms by which alkali metal nonstoichiometry is accommodated. Barium hexaaluminate and hexaferrite are both highly ordered. Specimens prepared by the borate flux method exhibit a new $\sqrt{3}a \times \sqrt{3}a$ superstructure of the hexagonal magnetoplumbite cell.

HREM images of $La_2NiO_{4+\delta}$ do not show evidence for the existence of higher homologues of the $La_{n+1}Ni_nO_{3n+1}$ family. Images of the $n = 2$ ($La_3Ni_2O_7$) and $n = 3$ ($La_4Ni_3O_{10}$) members of the family occasionally show the presence of higher members. Images of ordered $n = 2$ and 3 members of this family have also been obtained.

In the $(NaCa)_nNb_nO_{3n+2}$ system ($4 < n < 4{\cdot}5$), ordered intergrowth structures are observed in samples prepared from $Ca_2Nb_2O_7$ and $NaCa_4Nb_5O_{17}$ or $NaNbO_3$, whereas random intergrowths are observed in samples prepared from Na_2CO_3, $CaCO_3$ and Nb_2O_5. Different ordered intergrowths are energetically similar as evidenced by the occurrence of different structures in a single preparation of $n = 4{\cdot}33$ or in the formation of polytypes of a given composition.

Monophasic solid solutions of the type $W_{1-x}Mo_xO_3$ have been prepared by the topotactic dehydration of the monohydrate, $W_{1-x}Mo_xO_3 \cdot H_2O$. A new form of MoO_3, in ReO_3-like structure, prepared by the *in-situ* dehydration of $MoO_3 \cdot H_2O$ has been characterized. An HREM investigation of the reduced oxides of the type $W_{1-x}Mo_xO_{3-\delta}$ ($\delta = 0{\cdot}05 - 0{\cdot}15$) has helped us in identifying three composition regions, $0{\cdot}3 < x < 0{\cdot}6$; $0{\cdot}60 < x < 0{\cdot}70$ and $0{\cdot}05 < x < 0{\cdot}3$ with distinct structural characteristics. For $0{\cdot}3 < x < 0{\cdot}6$, the system shows randomly oriented {102} crystallographic shear (cs) planes. For $0{\cdot}05 < x < 0{\cdot}3$, the cs planes did not precipitate, formation of a domain structure seems to accommodate oxygen deficiency in this range. The varied behaviour in the different composition ranges of $W_{1-x}Mo_xO_{3-\delta}$ has been attributed to the preferential reduction of molybdenum in the solid solutions.

Potassium bronzes of the type $K_yW_{1-x}Mo_xO_3$ formed by the $W_{1-x}Mo_xO_3$ solid solutions have been prepared for the first time. Mo-rich compositions ($x \simeq 0{\cdot}7$) form HTB-like phases for $0{\cdot}10 < y < 0{\cdot}15$, and a blue-bronze phase for $y = 0{\cdot}4$. W-rich compositions form only HTB-like bronzes for $0{\cdot}2 < y < 0{\cdot}33$

References

1. RAO, C N R — In *Materials for solid state batteries*, (eds) B V Chowdari and S Radhakrishna, 1986, p 3, World Scientific
2. RAO, C N R AND GOPALAKRISHNAN, J — *New directions in solid state chemistry*, 1986, Cambridge University Press
3. RAO, C N R — *Sadhana*, 1988, **13**, 19–35
4. MOHAN RAM, R A, GANAPATHI, L GANGULY, P AND RAO, C N R — *J Solid St Chem*, 1986, **63**, 139–147
5. BHAT, V AND GOPALAKRISHNAN, J — *J Chem Soc Chem Commun*, 1986, 1644–1645
6. GANAPATHI, L, SUBBANNA, G N, GOPALAKRISHNAN, J AND RAO, C N R — *J Mater Sci*, 1985, **20**, 1105–1110.
7. ER-RAKHO, L, MICHEL, C, PROVOST, J AND RAVEAU, B — *J Solid St Chem*, 1981, **37**, 151–156

Thesis Abstract (M.Sc. (Engng))

A study of the effect of strakes on the vortical flow past an upswept aftbody by Munshi Sandeep Ranjankumar.
Research supervisor: S. P. Govinda Raju.
Department: Aerospace Engineering.

1. Introduction

Modern military transport aircraft employ aft loading of cargo and thus need a fuselage with a highly upswept aftbody (as in the case C-130, Hercules and C-5A, Galaxy aircraft) The resulting shape of the aftbody deviates considerably from an ideal streamlined body As a result, the forebody boundary layer approaching the aftbody is thick and turbulent and separates with a shedded vortex pair, similar in many respects to that on a delta wing at large incidence. This vortex pair located below the bottom of the upswept aftbody induces suction which causes an inclined load to act on the aftbody There is thus a contribution to drag from this inclined load which adds to the cruise drag of the fuselage considerably Further, the negative lift on the aftbody produces an undesirable nose-up pitching moment

The importance of reducing cruise drag of an aircraft can be appreciated from the estimates of payload gain due to drag reduction. Estimates show that a decrease of 0·4% of cruise drag coefficient increases the payload of a long-range transport aircraft by about 1% Typically, the fuselage contribution to aircraft drag is about 25% Thus a 5% decrease in fuselage drag results in a payload gain of about 3% It appears possible to reduce the fuselage drag by about 5% by controlling the aftbody flow and the potential gain in payload is thus very significant

Analytical and computational methods are still not powerful enough to study the above problem because of the complexity of the three-dimensional separated flow. As a result, only experimental studies are feasible and there have been a few earlier such studies[1–4] Flow visualisation studies by Wickens[1] and Peake[2] clearly show the existence of a vortex pair below the aftbody bottom surface. Some flow-control devices like strakes and flow deflectors appear to have been tried with some success, but details of these are not available in published literature This work is an attempt to fill this gap by a systematic experimental study.

A typical upswept aftbody model has been designed and fabricated for this study. To measure the relatively small aerodynamic forces on the model (of the order of 2N), a special-purpose three-component balance has been designed and fabricated Strakes of various sizes attached to the aftbody have been tested for their effectiveness in controlling the vortical flow. Effect of strake parameters like chord, span, location and orientation have been systematically studied and an optimal strake configuration resulting in about 6% reduction of drag has been obtained.

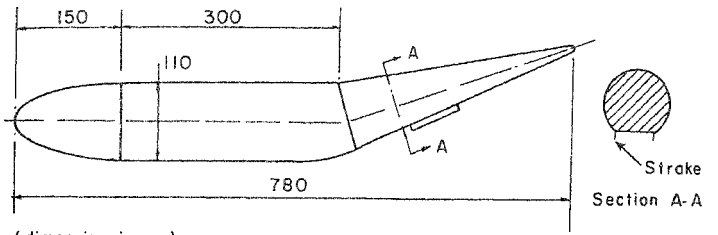

FIG 1 Model of fuselage with upswept afthody (dimensions in mm)

2. Experimental set-up and instrumentation

A low-speed wind tunnel, 0 5 × 0 5m test section, available at the Indian Institute of Science, has been used for the present study The maximum wind speed in the test section is about 25 m/s resulting in a test Reynolds number for the model of about one million based on its length. The model is about 110 mm in diameter resulting in a blockage ratio of about 4% of test section area which is adequately small.

The model geometry is based on a typical upswept fuselage of a military transport aircraft (Fig 1) It has a semi ellipsoidal nose, a cylindrical forebody and an afthody with its centre line upswept by 18 degrees It is fabricated by attaching wooden nose and aft sections to the cylindrical centre section cut from a plastic tube. The bottom portion of the afthody is flat all the way to the end A 10-mm wide strip of semirough emery paper has been glued around the base of the wooden nose to obtain a turbulent boundary-layer downstream. The model is suspended into the test section from a platform balance located on top of the test section by two rods. Strakes of various sizes are glued to the afthody as required.

The aerodynamic forces on the model during the tests are small, typically 1 N. To measure the small forces accurately so that one can resolve the small influence of the strakes, it was necessary to develop a new balance system. The balance can measure lift, drag and pitching moment on the model located in the test section The outputs from the balance are electrical signals of the order of a few millivolts and are measured using digital voltmeters

The balance (Fig 2) consists of a light rectangular platform measuring 300 × 330 mm suspended from a horizontal supporting plate by three steel wires of about 0 35 mm in diameter The model located in the middle of the test section with its symmetry plane horizontal is connected to the platform by two suspension rods. Thus, the aerodynamic forces to be measured all lie in horizontal plane and are transferred to the platform, which is constrained by three strain-gauged cantilever beams attached to the platform by means of long horizontal connecting rods. The electrical outputs from the strain-gauge beams are linearly related to the aerodynamic forces, the relation being obtained by an *in-situ* calibration using dead weights.

The rods attaching the model to the platform can be fixed at various positions in slots in the form of circular arcs cut in the platform so that the model can be rotated within limits about a vertical axis thus varying its angle of attack over range of ± 15 degrees The whole arrangement, consisting of the balance and its support structure, is enclosed by a pressure-tight cover to prevent any airflow into the test section which is at less than atmospheric pressure during operation

The balance is designed and fabricated such that of the three links constraining the platform, one is parallel to the tunnel axis while the other two are at right angles to it, thus ensuring negligible interaction between axial and lift force measurements However, the interactions are accounted for during calibration and use of the balance. Actual dead-weight calibration *in situ* has shown that the calibration matrix is

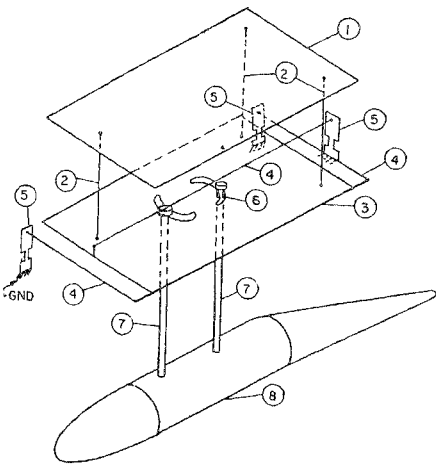

1 Supporting plate
2. Suspension wires
3 Metric platform
4 Connecting links
5 Strain-gauged beams
6 Slots for α variation
7. Rods for model support
8 Model

FIG. 2 Schematic layout of 3-component balance

$$\begin{bmatrix} A \\ N1 \\ N2 \end{bmatrix} = \begin{bmatrix} 145{\cdot}5 & -1{\cdot}2 & 1{\cdot}8 \\ -0\,7 & 150\,0 & -0{\cdot}4 \\ 2{\cdot}7 & 2{\cdot}0 & 153{\cdot}4 \end{bmatrix} \begin{bmatrix} R1 \\ R2 \\ R3 \end{bmatrix}$$

This matrix clearly indicates that the off-diagonal terms representing interactions are less than 2·0% compared to diagonal terms and are thus very small.

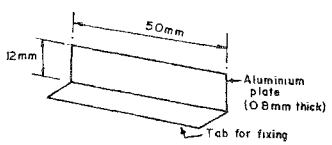

FIG 3. A typical stake

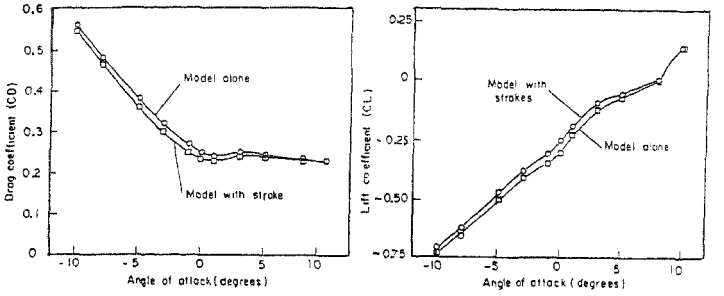

FIG 4. Comparison of force coefficients with and without strakes

3. Results and discussion

A systematic parametric study involving various parameters like strake chord, span, axial position on the fuselage aftbody, orientation relative to fuselage axis and angle of attack of the model has been carried out to assess the effectiveness of strakes in controlling the vortical separated flow. The strakes were made of 0·8-mm aluminium plate of rectangular shape and were glued to the aftbody using integral tabs. Strake chords of 35, 50 and 65 mm were considered, and strake spans of 9, 12 and 15 mm were used. The mid-point of the strake was located at 50, 60 and 70% of the distance from the aftbody. Figure 3 shows a typical strake configuration.

The model was first tested without any strakes over an angle of attack range of about ± 10 degrees to determine the aerodynamic force coefficients for the clean configuration. All other configurations were tested over the same angle of attack range and the results compared with the results of the clean configuration (Fig. 4). The results indicate that there are several strake configurations yielding a reduction in drag coefficient and simultaneous reduction in the magnitude of the lift coefficient. This clearly indicates that strakes are effective in controlling the vortical flow. Within the limits of this study, the optimal strake span was 12 mm and the chord 65 mm. Location of the strakes with centre at 50% of the length along the aftbody resulted in maximum reduction in CD of around 6% compared to the clean configuration. Further, the reduction in drag is sustained over a fair range of angle of attack around 0 degrees and thus implies a worthwhile drag reduction for a realistic fuselage in the cruise configuration.

4. Conclusions

The possibility of reducing drag of an upswept aftbody by the use of strakes has been considered. A balance which can accurately measure small changes in force due to strakes on the aftbody has been successfully designed and used in the study. It has been shown that a significant reduction in the drag of the aftbody can be achieved by the use of strakes.

Notation

CD : Drag coefficient based on forebody cross-section area

CL : Lift coefficient

CM : Moment coefficient

C : Strake chord, mm

B : Strake span, mm

A : Axial force on the balance, N

N1 Normal force on the balance, N, at the first beam
N2 : Normal force on the balance, N, at the second beam
R1 . Output of axial force bridge, mV/V
R2 : Output of N1 bridge, mV/V
R3 · Output of N2 bridge, mV/V

References

1 WICKENS, R H *Aeronautical Report*, LR-395, National Research Council, Canada, Jan 1964
2 PEAKE, D J *CASI J*, 1969, **15**(10), 399–408
3 KOLESAR, C E AND MAY, F W *AIAA paper* 83-1787, 1983
4 HALLSTAFF, T H AND BRUNE, G W *AIAA paper* 84-0614, 1984

Thesis Abstract (M.Sc. (Engng))

Studies on the kinetics of catalytic methanation of carbon dioxide by G. M. Shashidhara.
Research supervisor: M. Ravindram.
Department: Chemical Engineering.

1. Introduction

Hydrogenation of carbon dioxide and carbon monoxide, when present together, is of much practical interest because of its application in catalytic gas purification[1], especially in synthetic ammonia production. Considerable amount of work has been reported on catalytic hydrogenation of carbon monoxide compared to that of carbon dioxide Also, most of the reported work on CO_2 hydrogenation is restricted to the temperature range of 200–400°C. On the other hand, increased demand for energy has resulted in an interest in catalytic conversion of CO to CH_4 and higher hydrocarbons, and also in a search for new carbon sources which could be converted into hydrocarbon fuels As many countries have large fields of natural carbonic acid[2], CO_2 can be regarded as a potentially cheap source of carbon.

2. Present investigation

Heterogenous catalytic methanation of CO_2 has been investigated with a view to study the kinetics of this reaction at atmospheric pressure over relatively higher temperature range of 320–516°C. Nickel–alumina and ruthenium–silica catalysts employed in this study were found to yield selectively CH_4 but neither CO nor CH_3OH as noticed by some previous workers[3-4] The stoichiometric equation which represents this reaction is

$$CO_2 + 4H_2 \rightarrow CH_4 + 2H_2O.$$

A detailed thermodynamic analysis of this reaction revealed large negative values of free energy change ($\Delta G^0_{298} = -27{\cdot}15$ kcal/mol) and high-value equilibrium constant ($K = 0{\cdot}8187 \times 10^{20}$ at 298K) thereby indicating the feasibility and irreversible nature of this reaction. The reaction was found to be fairly exothermic ($\Delta H^0_{298} = -39{\cdot}43$ kcal/mol) and the variation of the heat of reaction with temperature in the range 593–789 K was negligible. Maximum possible conversions at 789 K for nine different feed ratios of CO_2 and H_2 varying between 1:4 and 1.11 were calculated. A considerable increase in conversion with mole ratios was noticed up to a mole ratio of 1:8 and the effect was negligible for larger ratios.

The nickel catalyst supported on alumina was prepared by conventional impregnation technique. The catalyst which was in oxide form was reduced *in situ* in the reactor with a slow stream of H_2 at the highest reaction temperature Surface area of the support and the catalyst were determined by both BET and liquid

adsorption (EGME) methods. Specific surface area of the Ni-Al_2O_3 catalyst was found to be 74·09 m^2/g. Analysis of the catalyst has shown that it contained 7·77% nickel. Ru-SiO_2 catalyst was obtained from the Indian Institute of Technology, Bombay

3. Experimental

The experiments were conducted in a circulating flow apparatus at atmospheric pressure which mainly consisted of a feed unit, a stainless steel micro reactor and a product collection unit. Reactant gases drawn from high-pressure cylinders were purified, metered and preheated before they were fed to the reactor. The reactor was heated externally by Kanthal heating wire and the desired temperature was housed inside the reactor between two plugs of glass wool. Products leaving the reactor were cooled, condensed and the moisture-free product stream was collected over saturated brine in a gas sampler for analysis purposes. Gas chromatographic analysis of this sample employing a Porapak-Q column and thermal conductivity detector system operated at room temperature showed that it contained only CH_4 and unreacted CO_2 and H_2. CO_2 content was crosschecked by Orsat analysis. The feed mixture was analysed before each run. In a typical analysis, H_2 and CO_2 contents in the feed, estimated by gas chromatograph/Orsat apparatus and also calculated based on flow meters, were found to be in good agreement. Before starting the kinetic experiments, the following preliminary experiments were conducted.

1. Material balance in the absence of catalyst,
2. Material balance in the presence of catalyst,
3. Activity of the catalyst,
4. Effect of external diffusion,
5. Effect of temperature on conversion, and
6. Effect of time factor on conversion.

From these experiments, it was found that there was no leakage in the apparatus and CO_2 was transformed only to CH_4. The nickel–alumina catalyst showed a constant activity after three hours when contacted with the reaction mixture at 658K and remained constant up to 10–12 hours. External diffusional resistance was found to be negligible for total flow rates in excess of 15.4 l/h. The extent of internal diffusional resistance was calculated for the catalyst of particle size ~ 150 + 170 Tylor series, by Weisz-Prater criterion, and was found to be negligible. Absence of inter- and intraparticle temperature gradients over the conditions employed in our experiments was further supported by calculating the necessary parameters, given in any standard textbooks on heterogenous catalytic reaction. Based on the preliminary experiments, reaction conditions for the actual kinetic runs were selected. With 0·5696 g of nickel–alumina catalyst, kinetic data were collected in the form of conversion as a function of time factor at five different temperatures, *viz*, 593, 649, 705, 761 and 789K. Time factors were varied between 0·96 and 3·87 g h g mol^{-1}. A constant feed mole ratio of 1·11 (CO_2:H_2) was maintained in all the experiments. A feed mole ratio of 1:7·15 was employed with ruthenium–silica catalyst. Employing 0·1301 g of ruthenium–silica catalyst, experiments were conducted at five temperatures, *viz.*, 593, 623, 649, 705 and 733K while the time factor was varied between 0·15 and 0·82 g.h g mol^{-1}. The maximum conversions observed were 98·59 and 26·5% with nickel–alumina and ruthenium–silica catalysts, respectively.

4. Discussion

For a quantitative description of these results, a power law type rate expression was derived in the present case by the order of reaction approach. Since the feed contained a large excess of hydrogen, it was reasonable to assume that the reaction rate depends only on the limiting reactant, *i.e.*, CO_2. It was proved in the present case that the reaction was first order with respect to CO_2. Plots of $\int_0^f df/-r$ *vs* W/F_{CO_2} yielded linear plots with zero intercept. Reaction velocity constant at different temperatures was evaluated from the slopes of these linear plots. The temperature dependence of reaction rate was assessed by applying Arrhenius equation. Values of activation energy calculated by the method of least squares were found to be 8·503 kcal/mol and 8·859 kcal/mol for nickel–alumina and ruthenium–silica catalysts, respectively. The validity of the rate expressions was checked by evaluating the values of conversion at known time

factors and temperatures. These values were found to be in good agreement with an average deviation of −4·82 and −4·71% for nickel–alumina and ruthenium–silica catalysts, respectively

References

1 VLASENKO, V. M., YUZEFORICH, G. E. AND RUSOV, M. T. *Kinet. Katal.*, 1965, 6, 849–851

2 SOLYMOSI, F., ERDOHELY, A AND KOCSIS, M. *J. Chem. Soc., Faraday Trans.*, 1981, 1, 1003–1012.

3 RAMAROSON, E., KIEFFER, R AND KIENNEMANN, A *J. Chem. Soc., Chem. Commun.*, 1982, 645–664

4 MOGGI, P., ALBANESI, G., PREDIERI, G AND SAPPA, E *J. Organomet. Chem.*, 1983, **252**, C89–C92

Thesis Abstract (M.Sc. (Engng))

Studies on the extraction of cobalt and nickel by di (2-ethyl hexyl) phosphoric acid by K. Ramesh Gupta.
Research supervisor: A. K. Mukherjee.
Department. Chemical Engineering.

1. Introduction

Organo-phosphorus acids form major section of extractants used for commercial extraction and separation of metals from dilute aqueous solutions Di(2-ethyl hexyl) phosphoric acid (abbreviated as D2EHPA in text and HA in formulae) is one of the outstanding members of this family of extractants.

Even though D2EHPA is a popularly used reagent for the extraction of cobalt and nickel, literature review shows that very little attention is paid to the understanding of mechanism and kinetics of extraction. The present study was made to understand the fundamentals of extraction of these metals by considering simple systems, obtaining equilibrium and kinetic data and evaluating the data to find the nature of the metal-extractant species, etc

2. Reagents, apparatus and procedure

D2EHPA, an AR-grade reagent of Fluka Chemicals, was used as received. All other salts and solvents were also of AR grade.

Organic phase was made of D2EHPA of appropriate concentration with toluene as diluent and 12% acetone as phase modifier. Aqueous phase with required metal concentration was prepared by dissolving appropriate amounts of sulfate salts of those metals in distilled water. pH was adjusted by adding concentrated sulfuric acid or liquor ammonia. Phase ratio in all the experiments was 1:1.

Equilibrium studies were conducted in separating funnels and kinetic experiments in the simplest form of the Lewis cell with single paddle-type stirrer The stirrer contained two sets of paddles, one dipped in the organic phase while the other in the aqueous phase, so that each phase can be stirred without disturbing the interface. Other types of stirrers with single set of paddles were also used to stir either of the phases as and when desired.

A uv-visible spectrophotometer was used for the analysis of cobalt and nickel. Cobalt was estimated by ammonium thiocyanate method and nickel by dimethyl glyoxime method.

3. Results and discussion

Equilibrium and kinetic studies were conducted in a wide range of experimental conditions.

3.1 *Equilibrium studies*

The simplicity of the system studied allowed to make some reasonable assumptions for the interpretation of the equilibrium data to find the extraction reaction. The assumptions are

(i) All the metal present in aqueous phase is present as M^{2+} ions

(ii) Concentration of the metal ion in the aqueous phase can be taken as a measure of activity of that ion in that phase

(iii) All D2EHPA in the organic phase will be in dimer form.

(iv) Change in extractant concentration due to extraction is negligible

With these assumptions the extraction reaction for a divalent metal ion can be represented by the following relation

$$M^{2+} + (1 + X)\ (HA)_2 = CoA_2 \cdot X(HA)_2 + 2H^+ \qquad (1)$$

where X is the number of HA molecules complexed to CoA_2

Equation (1) can be, after some simplifications, reduced to the form,

$$\log D + 2 \log[H^+] = \log K + (1 + X)\ \{\log (HA)_2\} \qquad (2)$$

where D is the equilibrium distribution coefficient and K the apparent equilibrium constant. Now the plot of $\log D + 2 \log[H^+]$ *vs* $\{\log(HA)_2\}$ should give a straight line with slope equal to $(1 + X)$.

It was observed that the value of $\log D + 2 \log[H^+]$ remained practically constant for particular $(HA)_2$ concentration, irrespective of the initial metal concentration in the aqueous phase. Averages of these values were taken and plotted against initial $(HA)_2$ concentration which gave a straight line with slope 2·5 in the case of cobalt and 3·0 for nickel. This indicated that the final metal-extractant complex and thus the overall extraction reaction for cobalt and nickel are different.

Based on these results the overall extraction reaction for cobalt and nickel can be written as

$$Co^{2+} + 2{\cdot}5(HA)_2 = Co(HA_2)_2 \cdot HA + 2H^+; \qquad (3)$$

$$Ni^{2+} + 3(HA)_2 = Ni\ (HA_2)_2 \cdot 2HA + 2H^+ \qquad (4)$$

Based on these overall extraction reactions and on the earlier works of Madigan[1] and Hughes and Zhu[2] separate schemes of reaction mechanisms were proposed for the extraction of cobalt and nickel.

3.2. *Kinetic studies*

Before going to actual kinetics studies, the regime of extraction was recognised by selective stirring of the phases and interpreting the results thereof. The conclusion was that the regime of extraction is situated at the organic side of the interface in both the cases of cobalt and nickel.

It was found by experiments that the effect of initial hydrogen ion concentration, in the range studied, is negligible on the kinetics of extraction. Subsequently, in all further experiments, initial pH of the aqueous phase was kept at 5·0 and the effect of pH was not considered in the discussion of results.

Extraction, in general, was very fast and the extraction *vs* time curves were very steep initially and flattened rapidly. More than 70% of the equilibrium extraction took place in about 4 minutes in most of the cases. Initial rates of extraction were obtained by curve fitting the data and differentiating it with respect to time $t = 0$. The initial rates thus obtained were used to calculate the apparent orders for metal ion concentration in the aqueous phase and D2EHPA concentration in the organic phase.

Following assumptions were made in addition to the ones made for equilibrium studies.

(i) Initial rate obtained by experiments are forward rates at that point of time

(ii) Initial rate is zero order with respect to hydrogen ion concentration under present experimental conditions.

With these assumptions the rate equation can be written as,

$$r_i = k\ C_M^a\ C_{(HA)_2}^b \tag{5}$$

where

r_i = initial rate of extraction of metal into the organic phase,

C_M = initial cobalt/nickel concentration in the aqueous phase,

$C_{(HA)_2}$ = initial D2EHPA concentration,

k = forward rate constant, and

a, b = orders with respect to metal concentration and D2EHPA concentration, respectively

At constant D2EHPA concentration in the organic phase, equation (5) reduces to

$$r_i = k_1\ C_M^a \tag{6}$$

so that

$$\log r_i = \log k_1 + a \log C_M. \tag{7}$$

Thus the plot of log r_i *vs* log C_M should give a straight line with slope equal to *a* which is the order with respect to metal ion concentration.

Similarly, for constant metal ion concentration in the aqueous phase, log r_i *vs* log $C_{(HA)_2}$ will give a straight line with slope equal to *b* which is the order with respect to D2EHPA concentration in the organic phase.

The values of *a* and *b* obtained by experiments are as follows

$a = 0{\cdot}5695$ and $b = 0{\cdot}8711$ for cobalt, and

$a = 0{\cdot}6169$ and $b = 1{\cdot}0490$ for nickel

The forward rate constant may be found by substituting these values in eqn (5).

References

1 MADIGAN, D C — *Aust J Appl Chem*, 1960, **13**, 58–66

2 HUGHES, M A AND ZHU, T — *Hydrometallurgy*, 1985, **13**, 249–264

Thesis Abstract (M.Sc. (Engng))

Studies on the diffusion coefficients of organic liquids by G. Ramprasad.
Research supervisors: T. R. Das and A. K. Mukherjee.
Department: Chemical Engineering.

1. Introduction

We report here the experimentally determined diffusion coefficients for the binary systems of benzene-, toluene- and xylene-alcohols. The alcohol series comprises the first eight members of the homologous series of paraffinic alcohols A correlation with simple physical properties of the diffusing species is obtained to calculate integral diffusion coefficients at any composition

2. Experimental

The diaphragm cell method[1] was used to measure the integral diffusion coefficients A G-4-grade

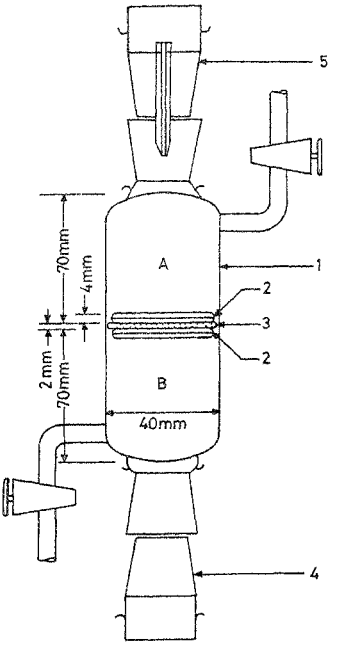

Scale 1:1

Item no.	Name	Specifications
1	Cell	Pyrex
2	Magnetic stirrers	Glass
3	Diaphragm	Porcelain no 4
4,5	Stoppers	Groundglass B-24

FIG 1. Diaphragm cell

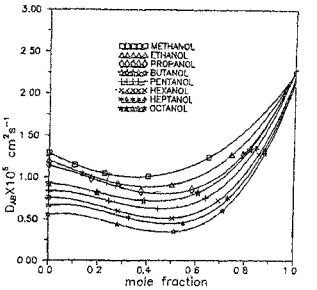

FIG. 2 Benzene-alcohols

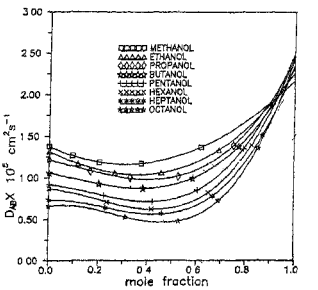

FIG 3 Toluene-alcohols

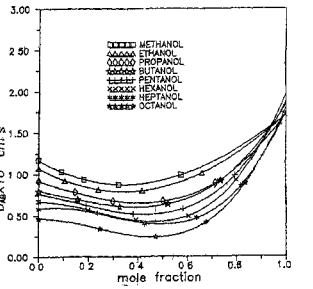

FIG 4 Xylene-alcohols

diaphragm was used in the present work (Fig. 1). The stirrers in the cells, made of iron wires embedded in glass, were rotated by the revolving bar magnets outside the cell

The diaphragm cell was calibrated at 298·15K by diffusing 0·1 molar potassium chloride solution into double-distilled water. From the known values of diffusion coefficients[2] for a range of concentrations of $KCl–H_2O$ systems at 298·15K, the cell constant β was calculated. With the cell constant thus known, the integral diffusion coefficient for any experimental system was calculated as

$$D_{AB} = \frac{1}{\beta t} \ln \frac{C_{i,B}\, C_{i,T}}{C_{f,B} - C_{f,T}} \tag{1}$$

where, $C_{i,B}$ and $C_{f,B}$ are the initial and final concentrations of the diffusing species in the bottom compartment and $C_{i,T}$ and $C_{f,T}$ the initial and final concentrations in the top compartment, and t the time of diffusion in seconds

The cell constant β remained almost unchanged after a period of 240 hours of usage, however, over a period of 960 hours of usage there was a 2·5% change in the value of the cell constant. The diaphragm cell was maintained at a temperature of 301·15 ± 0·5K with a thermostat bath in all the experiments

Each experiment was repeated twice and the agreement between the diffusion coefficients thus determined was within 5%. Error analysis indicated that the maximum possible error in the diffusion coefficient could be ± 14%

All the chemicals used were either spectro or guaranteed reagent grade

3. Results and discussion

For any system, a relation between the experimental integral diffusion coefficient and the composition of the mixture is obtained in the form of a third-order Chebyshev polynomial of the first kind. In this relation, four constants are obtained. The procedure is repeated for each of the other binary systems. Each of the four constants is related to a particular property in the form of a third-order Chebyshev polynomial of the first kind. The four properties (denoted by P_1 to P_4) used in these relations are given below

$$P_1 = [\, M_A^{0.5} + (\eta_B/\eta_A)^{0.6}] \,/\, [\, \eta_A + (V_B/V_A)^{0.6}] \tag{2}$$

$$P_2 = [M_A + (\eta_B/\eta_A)^{0.5}]/\eta_A \tag{3}$$

$$P_3 = [M_A^{0.5} + (\eta_B/\eta_A)^{0.55}]/\eta_A \tag{4}$$

$$P_4 = [M_A + (\eta_B/\eta_A)^{0.2}]/\eta_A \tag{5}$$

where M, η and V are the molecular weight, viscosity and molar volume, respectively

Figures 2–4 give the experimental and calculated diffusion coefficients for benzene-, toluene- and xylene-alcohols, respectively, for various compositions of the mixtures. In each diagram, experimental data are given by discrete points whereas continuous curves give the calculated values.

It is seen that as the viscosity increases from methanol to *n*-octanol there is a corresponding decrease in the value of the integral diffusion coefficient. The diffusion coefficient for any system first decreases with the molefraction, reaches a minimum and then attains a value which is constant for all the binaries of alcohol homologous series with an aromatic second component. This constant value is nothing but the self-diffusivity of the aromatic second component.

References

1 STOKES, R. H. Improved diaphragm cell for diffusion studies and some tests of the method. *J. Am. Chem. Soc.*, 1950, 72, 763–768

2 WOOLF, L. A. AND HARRIS, J. F. Revised values of integral diffusion coefficients of potassium chloride solutions for the calibration of diaphragm cells. *J. Phys. Chem.*, 1967, 71, 1962–1964

Thesis Abstract (M.Sc. (Engng))

Thermal decomposition of solids for energy storage by B. Venkata Ramana Murty. Research supervisor: M. S. Murthy.
Department: Chemical Engineering

1. Introduction

Thermal energy storage in packed beds is one of the methods for solar energy utilisation, for space heating and for low-temperature applications. The present investigation is an attempt to analyse the packed bed reactor. Heat-transfer characteristics of thermal energy storage system decomposition of calcium hydroxide is presented. Analysis of the packed bed reactor consisting of spherical pellets of calcium hydroxide and hot air at a temperature of 520°C was attempted.

The formulation of the problem consists of three stages. In the first stage, no chemical reaction takes place and the bed is heated by air, free of carbon dioxide and water vapor, till the solid reaches 400°C. In the second stage (> 400°C), thermal decomposition of calcium hydroxide takes place and heat of reaction is taken into account. In the third stage, *i.e.*, when the reaction is complete, the heat given by the fluid increases the temperature of the bed.

Equations describing the energy balance for fluid and solid mass in one dimension along the Z-axis have been presented for all three stages. Partial differential equations of the model have been solved for temperature profiles by finite difference technique in a stepwise manner starting from Z = 0·0 and marching upward till Z = H.

2. Experimental

The model was tested by carrying out the experiments in a cylindrical column packed with calcium hydroxide pellets. Temperature profiles were measured at three different heights in the reactor for three flow rates of air. The influence of chemical reaction rate has been studied in the second stage.

Volumetric heat-transfer coefficients have been evaluated from the experimental data and the effect of fluid velocity and inlet temperature on heat-transfer coefficients has been studied. Experimental values have been compared with the general correlations reported in literature.

An attempt has been made to analyse the decomposition of calcium hydroxide when chemical reaction controls the overall rate, taking density variations into account. It was found that the data for chemical reaction-controlled mechanism fits very well than the data excluding density variations.

Studies were also carried out on barium peroxide decomposition on thermogravimetric analyser. A non-isothermal model has been developed from the fundamental equations for the evaluation of kinetic parameters, and the effect of additives on the decomposition of barium peroxide studied.

The experiments were carried out in a Univac Sinku Riko thermomicrobalance. The samples used for analysis were made by physical mixing.

3. Results and conclusions

Theoretical time-temperature data compare satisfactorily with experimental data. From the results it is observed that temperature increases with increase in velocity of air and reduces the time required for the solid to reach the inlet temperature of the fluid. The rate expression required for the model was derived from the best fit equation obtained from the data of decomposition of calcium hydroxide pellets.

It is observed that aluminium is more effective than copper and zinc metal powders used as additives. It was also observed that there is a significant change in decomposition as the percentage of additive is increased. A two-step mechanism is proposed for the decomposition. Though copper is a better conductor than other metals, its presence was not found to be effective in lowering the decomposition temperature. This indicates that the decomposition may not be entirely heat transfer-controlled phenomena.

References

1 Beasely, D. E. and Clark, J. A. — *Solar Energy*, 1984, **32**, 314

2 Fujii, I. and Tsuchiya, K. — *Alternative Energy Sources – IV*, Vol. 1, 1983, p. 285

3 Murthy, M. S. — Technical report No. DST/SPD/46 (282)–80, 1984

4 Murthy, M. S., Raghavendrachar, P. and Sriram, S. V. — *Solar Energy*, 1986, **36**, 53–62

Thesis Abstract (M.Sc. (Engng))

Performance analysis and improvement of submersible pumps by P. Thanapandi.
Research supervisor: Ram Prasad.
Department: Civil Engineering.

1. Introduction

During the recent past, a number of methods have been introduced for analysing flow dynamics in turbomachines. One- and multi-dimensional flow analysis methods coupled with loss models have been used by many authors (for example, Colwill[1]) to predict the performance of ugal machines of varying specific speeds. The prediction procedures proposed so far successfully reproduce the test results mostly in a narrow region in the neighbourhood of the best efficiency point and the accuracy of the procedures for the low-flow region and the pumps of low-specific speeds is not high. This work describes a performance-prediction procedure, modelling all major losses likely to occur in the submersible pumps. Hence, it is applicable to the entire operating range.

2. Losses

2.1. *Impeller parasitic losses*

These losses occur outside the impeller and diffuser, and consist of (i) leakage loss due to flow through the clearance between impeller and casing, (ii) disk friction loss, and (iii) mechanical losses at the bearing and packing.

2.2. *Hydraulic losses*

These consist of losses due to skin friction, secondary flow and diffusion in the impeller and diffuser passages, wake mixing loss at vane outlet, shock loss at vane inlet and bend losses in diffuser passages.

All the above losses were estimated using loss models developed by various authors[2-8].

3. Performance prediction model

A prediction model incorporating the aforesaid loss models was developed for performance prediction of centrifugal pumps of low-specific speed operating at constant and variable speed. The main model is based on one-dimensional flow theory, and includes the calculation of boundary-layer thickness and its development through flow-passage blockage factor, jet-wake pattern analysis with establishment of separation criteria, etc., to make it applicable for low-specific speed machines.

The model performs three separate sets of computations at a series of discharges and speeds of rotation

which may be chosen to cover the whole range of probable operation of the pump. In the first set of calculations velocity triangle data are determined. The discharge is corrected for leakage and blockage is calculated taking into account the flow field distortion due to boundary layer development, separation and blade thickness. The theoretical head is calculated by Peck's method'. In the second set of calculations, losses in different components are arrived at. The third set of calculations makes the performance prediction. There is also provision for selection of optimum loss models among several alternatives based on test data. This, however, is not discussed further here.

The input to the model consists of fluid properties, speed of rotation and geometrical parameters of the components, viz., inlet and outlet diameter, passage width, blade thickness, blade angles, bearing clearances and length, wearing ring details, shroud thickness, etc., and the values for the empirical quantities in component loss models. The model outputs the efficiency and total head for the given discharge values and the magnitudes of the component losses in the operating range.

4. Experiments and measurements

Experiments for performance testing were conducted on a five-stage submersible pump of specific speed 32·9. The geometrical parameters of the impeller and casing for input into the model were measured with vernier calipers. The blade-angle profile of the shrouded impeller vane was obtained with radiograph techniques. The accuracy in measurement of all geometrical parameters is crucial, as error in measurements of sensitive parameters like impeller inlet-outlet diameter, width and vane angle have a great influence on the results.

5. Results and discussion

The performance prediction model was run with the geometrical data of the test pump. The predicted and experimental performance of the tested pump are shown in Fig. 1. The model results show good agreement with experimental data almost in the entire range of operation. There exists a difference between the predicted and test characteristics by nearly 2 per cent in low-flow range, *i.e.*, $0{\cdot}0 < Q / Q_D < 0{\cdot}3$, where Q_D is the best efficiency discharge and Q any other discharge. This shows that the actual head is somewhat underestimated and the efficiency values are overestimated by the model in this flow range. The underprediction of head and overprediction of efficiency values at low discharges may be attributed to errors in calculating circulation head and slip factor and their effect on the discharge flow angle. At low flows,

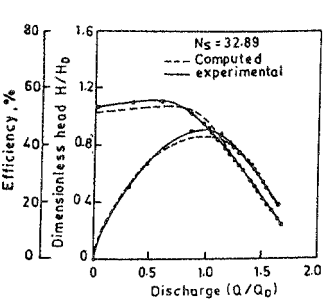

FIG 1. Comparison of predicted and experimental performance.

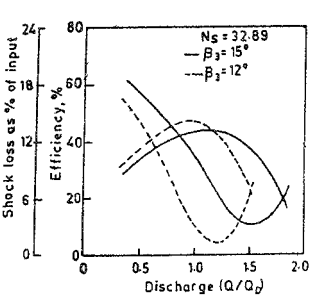

FIG 2. Performance improvement by correcting vane-angle mismatch

there is separation of flow from the suction surface. On the pressure side of the vanes, the flow will not deviate much from the vane surface, thereby resulting in reduction in the value of slip factor. Coriolis force and viscous effects on flow vortex, due to re-circulating flow, also cause reduction in slip factor. There is no provision in the present model to consider these effects. The one-dimensional boundary layer and blockage models have proved inadequate in the low-flow region and three-dimensional boundary layer technique can be expected to model this flow more satisfactorily.

Even with the discrepancies discussed above, the overall predictive capability of the model is generally excellent and the accuracy of prediction provides an indirect confirmation of accuracy of the detailed loss calculations.

The model can also be used to analyse the causes of poor performance of an existing pump. The behavior of the component losses at different flows often gives the required clue. For example, Fig. 3 shows the variation of shock loss with discharge for the pump whose characteristics are shown in Fig. 2. The minimum shock loss occurs at $1{\cdot}3Q_D$, while one expects it to occur around Q_D. This points to possible mismatch between the vane angles at impeller outlet and diffuser inlet. If the latter (β_3) is changed by 3°, the resulting shock loss and efficiency characteristics as predicted by the model (broken lines in Fig. 2) show that the efficiency increases by 4% and the minimum shock loss is not only lower than the earlier case, but is also closer to the best efficiency point.

References

1. COLWILL, W. H. — Impeller performance prediction using three-dimensional flow analysis, *Symp. on Performance Prediction of Centrifugal Pumps and Compressors*, ASME, Louisiana, March 1980.
2. TOYOKURA, T. AND KUROKAWA, J. — Axial thrust, disk friction torque and leakage loss of radial flow turbomachinery, *Int. Conf. Pump and Turbine Design and Dev.*, NEL, September 1976.
3. WILSON, J. N. AND GOULBURN, J. R. — An experimental examination of impeller passage friction and disk friction losses associated with high speed turbomachinery, *Int. Conf. Pump and Turbine Design and Dev.*, NEL, September 1976.
4. KARASSIK, I. J., KRUTZSCH, W. C., FRASER, W. H. AND MESSINA, J. H. — *Pump handbook*, 1976, McGraw-Hill.
5. NIXON, R. A. AND CAIRNEY, W. D. — *Scale effects in centrifugal cooling water pumps for thermal power stations*, NEL Report No. 505, April 1972.
6. MASHIMO, T. S., WATANABE, I. AND ARIGA, I. — Effects of Reynolds number on performance characteristics of a centrifugal compressor, with special reference to configurations of impellers, *Trans. ASME, A, J. Engng. Power*, 1975, **97**, 361–367.
7. GALVAS, M. R. — *Analytical correlation of centrifugal compressor design for maximum efficiency with specific speed*, NASA Technical Note, TN-D-6729, 1972.
8. MIZUKI, S., ARIGA, I. AND WATANABE, I. — Prediction of jet and wake flow within centrifugal impeller channel, *Symp. on Performance Prediction of Centrifugal Pumps and Compressors*, ASME, Louisiana, March 1980.
9. PECK, J. F. — Investigations concerning flow conditions in a centrifugal pump, and the effect of blade loading on head slip, *Proc. Instn. Mech. Engr.*, 1951, **1**, 164–165.

Thesis Abstract (M.Sc. (Engng))

Sensitivity and round-off noise studies on signal processor-based second-order digital filters by B. S. Prasanna.
Research supervisors: S. N. Rao and P. V. Ananda Mohan (ITI).
Department: Computer Science and Automation.

1. Introduction

Digital filters are invaluable tools for real-time signal processing because of their significant advantages

like accuracy, reproducibility and flexibility. Higher order digital filters are usually realized by cascading several second-/first-order structures. The general second-order digital filter transfer function contains two coefficients a, b which are realized by fixed or finite length binary words due to practical limitations. This leads to inaccurate representation of the coefficients and results in errors in the realized transfer function. Several authors have evaluated the errors due to such inaccurate representation by studying the movement of poles of the realized second-order digital transfer function[1, 2]. But such evaluation does not represent directly the sensitivity of the overall magnitude of the transfer function due to errors in representing the coefficient values.

2. Analysis and results

In this work, the fractional deviation in the overall magnitude of the transfer function $\Delta\,|H|\,/\,|H|$ is used as figure of merit for evaluation and comparison of various second-order digital filter structures

$$\Delta\,|H|\,/\,|H| \quad \cdot \; S_a^{|H|}\;(\Delta a/a) + S_b^{|H|}\;(\Delta b/b)$$

The evaluation is restricted to those structures which realise the coefficients using only two multipliers c, d.

Thus, we have

$$(\Delta a/a) \cdot S_c^a\,(\Delta c/c) + S_d^a\,(\Delta d/d);$$
$$(\Delta b/b) \cdot S_c^b\,(\Delta c/c) + S_d^b\,(\Delta d/d).$$

The evaluation of $\Delta\,|H|\,/\,|H|$ involves computation of several sensitivities $S_a^{|H|}$, $S_b^{|H|}$ which are structure independent and $S_{c,d}^a$, $S_{c,d}^b$ which are structure multiplier dependent.

A computer-aided sensitivity analysis procedure has been developed and used to evaluate and compare various structures. Some of the structures considered are systematically derived by replacing the delay blocks in direct form structure with first-order lossy and lossless integrators of various types, all pass networks and structures based on forward or backward Euler integrator types. Some among these have been described in literature previously by Yan and Mitra[5], Szczupak and Mitra[6,7], Gray and Markel[2], Fleischer and Laker[8] (switched capacitor) and Agarwal and Burrus[9]. Further, alternate realizations for direct form structures such as Agarwal–Burrus are also available. All these have been considered in the analysis using a FORTRAN computer program. The analysis described above can be applied to choose the 'best' structure for realizing a given transfer function.

Another important aspect in digital filter implementation is the evaluation of the effect of round-off invariably present during signal processing. The earlier methods of digital filter implementation used hardware multipliers and accumulators which provide the flexibilty for selecting a suitable word length to meet the sensitivity specifications. However, the current technique of implementation of digital filter structures uses digital signal processor chips. This imposes a restriction of fixed word length for realizing the coefficients. Hence, the round-off noise is dependent on the digital signal processor architecture. Thus, the systematic evaluation of round-off noise involves identification of noise sources in each structure and evaluation of their transfer functions to the output. Since the noise-transfer function can be of a general biquadratic type, a formula for round-off noise variance amenable to computer-aided evaluation has been derived. Sensitivity and round-off noise behaviour of various structures have been studied for a representative set of pole positions, five close to the unit circle and five well within the unit circle. Computer results for these cases have been indicated in the work to highlight the differences in the behaviour of various structures.

The procedures and techniques developed help the designer to choose an appropriate structure for the intended application.

References

1. GOLD, B. AND RADER, C. M — *Digital processing of signals*, 1969, McGraw-Hill
2. GRAY, A. H. AND MARKEL, J. — Digital lattice and ladder filter synthesis, *IEEE Trans*, 1973, **AU-21**, 491–500

3	OPPENHEIM, A V AND SCHAFER, R W	*Digital signal processing*, 1975, Prentice-Hall
4	RABINER, L R AND GOLD, B	*Theory and applications of digital signal processing*, 1975, Prentice-Hall
5	YAN, G T AND MITRA, S K	Modified coupled form digital filter structures, *Proc IEEE*, 1982, **70**, 762–763
6	SZCZUPAK, J AND MITRA, S K	On digital filter structure with low coefficient sensitivities, *Proc IEEE*, 1978, **66**, 1082–1083
7	SZCZUPAK, J AND MITRA, S K	Minimization of coefficient sensitivities of digital filter structures, *Proc IEEE*, 1979, **67**, 180–181
8	FLEISHER, P E AND LAKER, K R	A family of active switched capacitor biquad building blocks, *Bell Systems Tech J*, 1979, **58**, 2235–2269
9	AGARWAL, R C AND BURRUS, C S	New recursive digital filter structures having very low sensitivity and round-off noise, *IEEE Trans*, 1975, **CAS-22**, 921–927

Thesis Abstract (M.Sc. (Engng))

Application of exponential power estimator for speech coding by George Mathew.
Research supervisor: A. P. Shivaprasad.
Department: Electrical Communication Engineering.

1. Introduction

The transmission, storage and processing requirements of any signal, in general, and of speech, in particular, is largely dependent on its representation Digital representation of coding of speech has become very popular due to its advantages such as ruggedness to noise, efficient signal regeneration, ease of encryption, storage and retrieval, use of digital computers for processing, etc , over analog representation However, in digital coding, the price paid for these benefits is the increased bandwidth Hence, the main objective of digital coding of speech is to represent (encode) it in such a way that the encode speech bandwidth (bit rate) is minimum for a specified quality of reproduction In speech coding, it is known that the differential pulse code modulation (DPCM) schemes lead to a reduction of bandwidth requirement (by removing the redundancy) as compared to pulse code modulation (PCM) schemes, for a specified speech quality To achieve adequate dynamic range and good subjective speech quality, however, it is necessary to adapt the parameters of the quantizer and predictor to the input signal characteristics Several algorithms have been developed for adapting the quantizer and predictor, most of which suffer from high computational complexity and are not easily implementable

However, two points are noteworthy· firstly, variance estimation of the quantizer input forms the basis of adaptive quantization and secondly, in predictor adaptation using the least mean square gradient (LMS) algorithm it is the estimation of the reconstructed signal power which is important[1,2] Hence, it is possible to reduce the computational complexity of the APCM and ADPCM systems by resorting to computationally simple power estimation schemes The study reported here is concerned with the development of adaptive PCM and DPCM (APCM and ADPCM) systems which are based on computationally simple adaptive quantization and prediction algorithms.

The above-mentioned computational simplicity is achieved here by implementing the adaptation algorithms for the quantizer and predictor using the exponential power estimation technique (EPE) which is a modified form of an existing power estimation method[3]. The three important features of the EPE technique are: (a) the process of estimation does not involve any multiplication or division, (b) use of this power estimate leads to further reduction in the computational complexity since the estimate is expressed as a power of 2 (2^t, t being an integer), (c) sufficiently fast response rate due to its exponential nature, and (d) very easily controllable response rate. Hence, the use of EPE leads to a significant reduction in computational complexity.

2. Results and discussion

Comparative studies of EPE with two conventional power estimation schemes (block and recursive power estimators BPE and RPE) have been done in the context of step response, spectral parameter identification (of a second-order stationary stochastic signal) and adaptive prediction of speech (using different prediction orders) The results indicate that EPE is much superior to RPE and identical to BPE in performance However, the performance of EPE is limited by the finite number of distinct power estimate values which the EPE estimate is allowed to take It is significant to note that in spite of this limitation, EPE gives a performance which is computationally advantageous and on par with the computationally complex power estimation schemes

The adaptive quantizer used in the APCM and ADPCM systems is of the hybrid type[4] The reason for choosing the hybrid scheme instead of the instantaneous or syllabic scheme is to make the best use of the available finite number of quantizer step sizes, as the hybrid approach makes the instantaneous step size to vary in an optimum range as decided by the syllabic information of the input signal EPE is used to estimate the instantaneous and syllabic standard deviations of the quantizer input signal, for the purpose of adaptation To make the quantizer robust to transmission errors, a leakage mechanism has been introduced in the EPE algorithm Performance evaluation study of these systems has been done under noise-free and noisy channel conditions using uniform and nonuniform quantizing characteristics at different bit rates (16, 24 and 32 kilobits per second) The input signals used are sinusoidal, correlated Gaussian sequence and digitized speech sentences Segmented signal-to-noise ratio is the performance measure used

The APCM systems simulated at bit rates 24 and 32 kbps using the EPE-quantizer (EPEQ) provide almost identical performance as that of robust adaptive quantizer (RAQ)[5] for speech input while the performance degrades for sinusoidal input (due to the speech-specific design of EPEQ). Noisy channel performance study has been done at the bit error rates of 10^{-5}, 10^{-4}, 10^{-3} and 10^{-2} for speech and correlated Gaussian inputs. The EPE-based APCM is found to give almost similar performance as the RAQ-based APCM.

A detailed performance evaluation of the ADPCM system is done by introducing EPE into the quantizer and predictor adaptation algorithms, stage by stage Having recognized the limitation in the quantizer performance, imposed by the finite dictionary of step sizes, the quantizer algorithm is modified to increase the number of distinct step sizes. Further modifications are done to improve the dynamic range and noisy channel performances of the quantizer This study led to the conclusion that the EPE-based ADPCM is best suited for low bit rate applications At 16 kbps, this system outperformed the two conventional ADPCM systems considered (one using the RAQ and the block power estimator-based LMS algorithm) for comparison purpose, with the computational advantage of having $(3N + B + 1)$ multiplications and one division compared to the first system and $(B + 1)$ multiplications compared to the second system, where N is the predictor order and B the number of bits/sample However, EPE requires one extra exponential operation

References

1 COHN, D L AND MELSA, J L — The relationship between an adaptive quantizer and a variance estimator, *IEEE Trans*, 1975, **IT-21**, 669–671

2 WIDROW, B, MCCOOL, J M, LARIMORE, M G AND JOHNSON, C R JR — Stationary and nonstationary learning characteristics of the LMS adaptive filter, *Proc IEEE*, 1976, **64**, 1151–1162.

3 BELLANGER, M AND EVCI, C C. — An efficient step-size adaptation technique for LMS adaptive filters, *Proc IEEE Int Conf Acoustics, Speech and Signal Processing*, 1985, pp 1153–1156

4 NASR, M E M AND CHAKRAVARTHY, C V — Hybrid adaptive quantization, *IEEE Trans*, 1984, **COM-32**, 1358–1361

5 GOODMAN, D J AND WILKINSON, R M — A robust adaptive quantizer, *IEEE Trans*, 1975, **COM-23**, 1362–1365

Thesis Abstract (M.Sc (Engng))

Studies on metallic (Cu, Au and Mn) thin-film strain gauges by K. Rajanna
Research supervisor: S. Mohan.
Department: Instrumentation and Services Unit.

1. Introduction

The estimation of strain is a basic measurement in many branches of engineering and science Strain gauges are the common devices used for this purpose In addition to their fundamental use for measuring strain as such, strain gauges can be used for measuring other physical quantities such as loads, torques, pressures, vibration, etc They are used routinely especially in the quality control of various designs and experimental stress analysis work

The conventional types of strain gauges developed over the years are metallic wire, metallic foil and semiconductor strain gauges An important development in the field of strain-gauge technology[1] is the introduction of thin-film strain gauges Thin-film strain gauges offer a number of advantages over the conventional-type strain gauges The present work reports an attempt made in the direction of forming and study of thin-film strain gauges made of vacuum-deposited metal films It is aimed not only at studying the strain-sensitive behaviour of thin films, but also to make them as useful devices

2. Preparation of thin-film strain gauges

The various steps followed to prepare the thin-film strain gauges in the present work are a) Selection of suitable substrate, b) Thin-film deposition, c) Pattern formation, d) Deposition of the bonding pads and the protective overlayer, and e) Post-deposition heat-treatment for stabilization.

Mylar has been used as the substrate because of its attractive properties and ease of operation Films of copper, gold and manganese were prepared using resistive evaporation from a molybdenum boat The meandering path pattern[2] was adopted for the sensing film in the case of copper and gold. The required pattern formation was done using photolithography technique[3] However, for the less critical stage of depositing bonding pads, a mechanical mask was used SiO_2 protective overlayer was deposited using electron beam evaporation The thin-film strain gauges prepared were subjected to vacuum heat-treatment using the built-in radiant heating arrangement. Figure 1 shows the schematic of the thin-film strain gauge.

3. Results and conclusion

The resistance-strain characteristics of the gauges were studied using cantilever technique[4] The response

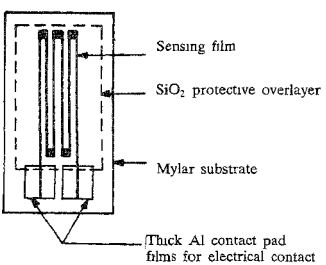

FIG 1 Schematic of the thin-film strain gauge

of the gauge with copper film as the sensing film to longitudinal and transverse strains in both tensile and compressive modes is discussed Similar behaviour was observed for the gauge with gold film[5] having meandering path pattern It is evident that the gauge response is linear in both the cases in tensile and compressive modes It is important to note that in tensile mode, $\Delta R/R$ is positive for longitudinal strains, whereas it is negative in the case of transverse strains This is attributed to the Poisson effect of sensing film grid lines Therefore, the gauge factor F_t for transverse strains turns out to be negative ($-0{\cdot}60$), and is much smaller compared to the gauge factor F_L (2·20) for longitudinal strains. A negative gauge factor for transverse strains was reported for silver film by Verma and Jain[6]

In addition to copper and gold film, the strain sensitivity of vacuum-deposited manganese films is also studied It is found that they exhibit linear response to strain. Compared to all other metals, manganese has the following advantages with respect to strain-gauge application.

(i) It has higher resistivity [185$\mu\Omega$-cm] Therefore, the gauge can have relatively higher resistance (without the meandering path pattern).

(ii) Its lower temperature coefficient resistance (TCR) makes it less sensitive to ambient temperature variation.

A study of the variation of gauge factor and TCR with thickness for manganese films shows that thicker manganese films possess gauge factor ~ 3 and TCR value around $3\,35 \times 10^{-4}$/°C

The thin-film strain gauges prepared are fairly smaller in size so that a better spatial resolution of the strain value can be obtained using these gauges They exhibit good linearity, stability and no noticeable hysteresis effect in their resistance-strain characteristics

References

1 PERINO, P R — Thin-film strain-gauge transducers, *Instrum Control Systems*, 1965, **38**, 119–121

2 RAJANNA, K AND MOHAN, S — Studies on meandering path thin film strain gauge, *Sensors Actuators*, 1988, **15**, 297–303.

3 GLANG, R AND GREGOR, L V — Generation of patterns in thin films In *Handbook of thin film technolgy* (L I Maisell and R Glang, eds), 1970, Ch 7, McGraw-Hill

4 SAMPATH, S AND RAMANAIAH, K V — Behaviour of Bi–Sb alloy thin films as strain gauges, *Thin Solid Films*, 1986, **137**, 199–205

5 RAJANNA, K. AND MOHAN, S — Longitudinal and transverse strain sensitivity of gold film, *J Mater Sci Lett*, 1987, **6**, 1027–1029

6. VERMA, B S AND JAIN, G C — Size effect in longitudinal and transverse strain coefficient of resistance in silver films, *Thin Solid Films*, 1972, **11**, 27–32

Thesis Abstract (M.Sc. (Engng))

Development and application of a new method for detection of structural equivalence in graphs/kinematic chains by K. Vijayananda.
Research supervisor: T. S. Mruthyunjaya.
Department: Mechanical Engineering.

1. Introduction

The kinematic structure of a mechanism is basic to an understanding of its function. The creative design of mechanisms involves the generation of kinematic chains having specified characteristics. Linear graphs have furnished a powerful tool for the analysis of kinematic chains In the graph representation of

kinematic chains, the links are represented by vertices, joints by edges, and the edge connection of vertices corresponds to the joint connection of links

To synthesize kinematic chains of a given class, a reliable and computationally efficient isomorphism test is needed Characteristic polynomial of the adjacency matrix of the chain is one index used extensively, and it has been found to fail in a number of cases[1-3] The existing isomorphism tests do not seem to meet the order of efficiency that the structural synthesis of kinematic chains demands. In this work, it is aimed to develop a new isomorphism test for simple and multiple jointed kinematic chains Representation set of the chain constitutes a new isomorphism index. The proposed test has been so tailored that it gives valuable information about the possible distinct mechanisms derivable from the chain. The effectiveness of the new test developed has been studied by incorporating it in an existing structural synthesis program

2. Representation set for chains/graphs

The index for isomorphism developed in the present work utilizes a graph-theoretic model of visual inspection The model has its basis in how one would visually comprehend the topology of a given graph in terms of the disposition of vertices and their interconnection by means of edges The systematic description of the given graph with reference to each of its vertices is expressed in the form of a set of rooted tree patterns By adhering to certain prescribed set of rules, each rooted tree pattern is eventually reduced to a number called the representation number. A set of such numbers, called the representation set, constitutes the isomorphism index for simple jointed chains/graphs The notion of a dummy link is introduced in the method while forming rooted tree patterns.

Multiple-jointed kinematic chains are uniquely converted into simple-jointed kinematic chains by introducing into the former a fictitious link at the location of joint multiplicity A suitable valency number is assigned to each fictitious link Representation set of the resulting simple-jointed chain constitutes the isomorphism index for multiple-jointed kinematic chain.

3. Derivation of distinct mechanisms

By using the representation set of the given kinematic chain, and the representation sets of the link-deleted subchains, it is conclusively shown that all possible structurally distinct mechanisms resulting from the chain can be derived.

4. Synthesis of 11-link, 2-d.o.f. kinematic chains

A computer program for structural synthesis and analysis of kinematic chains was developed by combining the new tests developed in the present work with an existing synthesis method based on the transformation of binary chains[4] Synthesis of 11-link, 2-d.o.f. chains showed that there are 839 structurally distinct simple-jointed chains of which 66 have total freedom, 86 possess fractionated freedom and the remaining 687 chains have partial freedom. A total of 7898 distinct mechanisms resulted from 839 chains. All the simple-jointed chains are displayed in the present work.

5. Results and conclusions

The isomorphism test based on representation set was successful in distinguishing all known kinematic chains and most of the counter examples which come under the general category of linear graphs However, the new test was unsuccessful to distinguish one pair of 15-vertex, 27-edge cospectral graphs. The CPU time taken to compute representation set of the chain varied from one-fifth to one-tenth the time required to calculate the characteristic coefficients of the adjacency matrix of the chain. The difference in the CPU time has been found to increase with the increasing number of vertices in the chain/graph. The new isomorphism test has been found to be flexible due to which some variations in the chain/graph can be conveniently handled Coding multiple-jointed kinematic chain is one such variation possible. Further study on the results of the synthesis of 11-link, 2-d o.f. chains revealed that there are 17 pairs and 1 triplet of kinematic chains which are non-isomorphic but have the same characteristic polynomial All these counter examples are presented in the work.

References

1 SCHWENK, A J — Almost all trees are cospectral, *New directions in the theory of graphs* (ed F Harary), 1973, Academic Press

2 READ, R C AND CORNEIL, D G — The graph isomorphism disease, *J Graph Theory*, 1977, **1**, 339–363

3 MRUTHYUNJAYA, T S AND BALASUBRAMANIAN, H R — In quest of a reliable and efficient computational test for detection of isomorphism in kinematic chains, *Mech Mach Theory*, 1987, **22**, 131–139

4 MRUTHYUNJAYA, T S — A computerised methodology for structural synthesis of kinematic chains, *Mech Mach Theory* 1984, **19**, 487–530